Reaction kinetics and rheological behaviour of meta-halloysite based geopolymer cured at room temperature: Effect of thermal activation on physicochemical and microstructural properties

Cyriaque Rodrigue Kaze, Thamer Alomayri, Assaedi Hasan, Sylvain Tome, Gisèle Laure Lecomte-Nana, Juvenal Giogetti Deutou Nemaleu, Herve Kouamo Tchakoute, Elie Kamseu, Uphie Chinje Melo, Hubert Rahier

Reaction kinetics and rheological behaviour of meta-halloysite based geopolymer cured at room temperature: effect of thermal activation on physicochemical and microstructural properties

Cyriaque Rodrigue Kaze[a,e,f*], Thamer Alomayri[b], Assaedi Hasan[c], Sylvain Tome[d], Gisèle Laure Lecomte-Nana[f], Juvenal Giogetti Deutou Nemaleu[e], Herve Kouamo Tchakoute[a], Elie Kamseu[e,**], Uphie Chinje Melo[a], Hubert Rahier[g]

[a]Laboratory of Applied Inorganic Chemistry, Faculty of Science, University of Yaoundé I, P.O. Box 812, Yaoundé, Cameroon.

[b]Department of physics, Umm-Al-Qura University, Makkah 21955, Saudi Arabia.

[c]Department of Physics, University College in AlJumum, Umm Al-Qura University, P.O. Box 715, Makkah 21955, Saudi Arabia; hsassaedi@uqu.edu.sa

[d]Department of Chemistry, Faculty of Science, University of Douala, P.O. Box 24157, Douala, Cameroon.

[e]Laboratory of Materials, Local Materials Promotion Authority, MINRESI/MIPROMALO, P.O. Box 2396, Yaoundé, Cameroon.

[f]Institut de Recherche sur les Céramiques (IRCER, UMRCNRS 7315), ENSIL-ENSC ENSCI, Université de Limoges, CEC, 12 rue Atlantis, 87068 limoges cedex, France

[g]Department of Materials and Chemistry, Vrije Universiteit Brussel, Pleinlaan 2, 1050 Brussels, Belgium.

Corresponding authors: kazerodrigue@gmail.com; cyriaque.kaze@uy1.uninet.cm; (Rodrigue Cyriaque Kaze); kamseuelie2001@yahoo.fr (Elie Kamseu);

Tel: 00237673259397/00237696963912; Fax: 00237222223720

Abstract

In this paper, four samples of meta-halloysite from widely available Cameroon halloysite clay calcined at 600, 650, 700 and 750 °C, respectively, and the resultant geopolymer binders were systematically characterized. Isothermal conduction calorimetry (ICC) was used to measure the reaction kinetics of meta-halloysite geopolymers at room temperature during 48h. The increase in reaction rate and in heat released correlates with the thermal activation temperature. It was typically found that the increase of thermal activation temperature (from 600 to 750 °C) enhances the amorphous or reactive phase content from MH600 to MH750 samples. This results in an improvement of rheological behaviour and setting time of the fresh meta-halloysite based geopolymer pastes. The hardened meta-halloysite based geopolymers were amorphous, compact and dense according to X-ray diffractometry (XRD) and Scanning Electron Microscopy (SEM). The compressive strength of resultant products increased with the activation temperature, up to 750 °C (74 MPa at 180 days). Therefore, the best temperature in view of the highest strength of meta-halloysite geopolymer cured at room temperature is 750 °C, although the lower increase in mechanical performance (7.3 %) gained between GPMH700 and GPMH750 is limited. Thus, thermally activated halloysite clay appears to be a promising candidate for geopolymer synthesis.

Keywords: Halloysite, thermal activation, meta-halloysite, kinetic reaction, rheology, geopolymer, mechanical properties

1. Introduction

Geopolymer binder is a rather new class of cementitious material resulting from a mixture of aluminosilicate powder with an alkaline or acid solution cured at a temperature less than 100°C (Davidovits 2015). Their structure consists of repeating units of Si-O-Al or Si-O-Si bonds, and are thus inorganic polymers. These materials attracted a lot of attention because of their interesting properties. Since about one decennium they find applications in several areas

such as construction and civil engineering, fire–resistant materials, insulation, various types of refractories, etc. (Leonelli *et al.* 2017; Yankwa Djobo *et al.* 2016; Bakharev 2006; Brachhold and Aneziris 2013; Tome et al. 2019). In literature, most papers on geopolymers deal with the precursors metakaolin, by-products resulting from power production and metallurgy (fly ash and slag), and some with volcanic ash (Kamseu *et al.* 2010; Provis and Bernal 2014; Vinai and Soutsos 2019; Patrick N. Lemougna *et al.* 2013). Particularly metakaolin has been studied, obtained from calcined kaolin clay known as 1/1 clay type, dehydroxylated between 550 and 800°C. However, few studies were carried out on halloysite which is a homologue 1/1 clay type. Halloysite is a two-layered clay and has a structure and chemical composition similar to that of kaolinite except for its higher water content (Hoffmann *et al.* 1934). The main difference is the shape of halloysite particles that can be platelet-like or tube-like depending on the pH value of the medium where it was formed (Yuan et al. 2012; Lecomte-Nana *et al.* 2017). Yuan et al. (2008) modified the surface of natural halloysite clay nanotubes with γ-Aminopropyltriethoxysilane (APTES) and compared the untreated and modified samples using characterization techniques such as nitrogen absorption, XRD, FTIR, TG/DTA, TEM and AFM. These authors found that the extend of modification is strongly affected by the morphological parameters of the original clay which demonstrated that the chemistry surface of halloysite nanotubes is readily modified, enabling applications in nanocomposites, enzyme immobilization and controlled release. Recently due to their superior thermal stability, high aspect ratios, biocompatibility, mechanical properties, and ease of availability, halloysite nanotubes exhibiting one dimensionality and hollow tubular nanostructures have attracted global interests due to their potential utilization in polymer nanocomposites (Idumah et al. 2019). In the West Region of Cameroon in Balengou locality, halloysite clay is widely available and can be valorized for the development of alternative binders (Pemunta *et al.*2014). Referring to chemical composition, silicon and aluminium oxides are the major

components present in halloysite thus rendering this aluminosilicate a possible candidate for the geopolymer synthesis (Zhang *et al.* 2016; Lázaro 2015). Several authors have thermally activated halloysite at different temperatures in order to produce geopolymers. Yuan et al. (2012) and Zhang et al. (2020) found that the halloysite crystals were completely destroyed and an amorphous phase was formed between 650 and 850 °C improving their reactivity in alkaline solution. Mackenzie *et al.* (2007) recommended a temperature of 800 °C to produce dehydroxylated halloysite from which geopolymers can be synthesized showing X-ray diffraction and Nuclear Magnetic Resonance (NMR), characteristics similar to that of metakaolin based geopolymer. Zhang *et al.* (2012) showed that kaolin containing some halloysite heated at 700 °C possessed higher Si and Al species dissolution rate than the purer kaolin and its metakaolin which improved their mechanical performances. Recently Kaze *et al.* (2018) produced geopolymer from Cameroon halloysite clay calcined at 600 °C mixed with silicates with different moduli (1.10, 1.25, 1.41 and 1.56) and the highest compressive strength of 27.5 MPa was reached at 1.25. Notwithstanding the satisfactory strength achieved, some residual halloysite was still present after the reaction, proving that after one hour at 600 °C the transformation of halloysite to meta-halloysite has not yet completed and that the remaining halloysite was not reactive enough. Bayiha *et al.* (2019) replaced calcined halloysite at 700 °C with limestone up 45 wt%. They found that the use of limestone as additive contributed in physical packing of the matrix leading to an improvement of mechanical properties. The authors mentioned above, obtained geopolymer binders from raw or calcined halloysite clays with various characteristics. From the literature it is well known that thermal activation is among the parameters which can affect the geopolymerization reaction from clayey aluminosilicate materials. Thermal activation was widely applied to kaolin clay for geopolymer synthesis and has shown a significant increase in final properties of resulting products (Rahier *et al.* 2000; Wang *et al.* 2010; Elimbi *et al.* 2011; Kenne *et al.*

2014). Compared to kaolinite, halloysite has higher specific surface areas due to their lower crystallinity induced by the insertion of water molecules which produces different basal spacings in their structure (Lazaro et 2015, Yuan et 2008, 2015; Zhang et al. 2020). This limited structural disorder that occurred in halloysite clay could be of great interest during the thermal activation of halloysite compared to that of kaolinite. This paper is the second in a series of articles describing the use of Cameroonian halloysite for the development of geopolymer binders. It was carried out with an objective to increase the reactivity of halloysite clay using thermal activation and compare the final properties of synthesized products to its homologue kaolin clay described in literature. The following temperatures 600, 650, 700 and 750 °C were used for thermal activation of halloysite clay. This work firstly deals with the effect of thermal activation on dehydroxylation of halloysite clay heated between 600 and 750 °C on the production of amorphous phase. Thus, the samples were tested by thermal analysis and thermogravimetric analysis (DTA/TG), X-ray diffractometry (XRD) and fourier transform infra-red spectroscopy (FTIR) in order to determine their mineralogical phases and dehydroxylation. Secondly to correlate the dehydroxylation temperature of halloysite clay to the reactivity, the reaction kinetics of geopolymerization and rheological behaviour of geopolymer binders resulting from halloysite clays calcined at different temperatures were monitored using isothermal conduction calorimetry (ICC) and rheometery. The characteristics of hardened meta-halloysite based geopolymer products are interpreted correlating the effect of thermal activation and development strength to the microstructure. Hence the effect of calcination temperature on physicochemical and mechanical properties of meta-halloysite based geopolymers cured at room temperature are reported and discussed with the purpose of finding the best calcination temperature of halloysite clay to synthesize geopolymer products with desired mechanical and microstructural properties.

2. Materials and methods

2.1 Materials

Halloysite clay used in this study was previously studied by Kaze *et al.* (2018) and represents about 80 wt% of halloysite clay. The chemical composition was 56.0 wt % SiO_2 and 29.3 wt % Al_2O_3. Whereas the mineral phases were halloysite ($Al_2Si_2O_5(OH)$, PDF #13-375); quartz (SiO_2, PDF #5-349); hematite (Fe_2O_3, PDF #13-5) and anatase (TiO_2, PDF #4-447). The halloysite clay was oven dried at 105 °C, ground and sieved at 80 µm. The resulting powders were calcined at 600, 650, 700 and 750 °C for 4 hours (heating/cooling rate 5.0 K/min) in a programmable electric furnace MIC (Muntatges Industrials per ceramic S.L type mini 51A N° 2350507). The obtained meta-halloysite powders were labeled MH600, MH650, MH700 and MH750. The sodium silicate solution used in this study was supplied by Ingessil s.r.l. Verona (Italy) and its chemical composition was; 14.37 wt% Na_2O, 29.54 wt% SiO_2, 56.09 wt% H_2O. Sodium hydroxide solution (10 M) was obtained by dissolving analytical grade sodium hydroxide pellets (BRAND) in distilled water. The alkaline activator was prepared by mixing of sodium hydroxide solution and sodium silicate solution with a mass ratio Na_2SiO_3/NaOH of 2.4 corresponding to final molar ratios SiO_2/Na_2O of 1.45 and H_2O/Na_2O of 10. The hardener was cooled and kept at room temperature for 24 h before using. This allowed the full depolymerization of sodium silicate in order to improve its reactivity.

2.2 Meta-halloysite geopolymer synthesis

The meta-halloysite geopolymer pastes were prepared by means of mixing the alkaline solution with each meta-halloysite powder according to a liquid/solid mass ratio of 0.83 used in our previous work (Kaze et al. 2018) in an automatic Hobart mixer for 5 minutes. This mass ratio allowed good workability of the paste. The geopolymer pastes obtained were then poured into cubic moulds (40x40 cm) and sealed into plastic bags to prevent water

evaporation. The moulded specimens were cured at 23±2 °C, and 98% relative humidity (RH). After 24 hours the cubic specimens were demoulded, covered with a thin film of polyethylene and stored at room temperature (23 ± 2 °C) and 98% RH. The cubic specimens labeled, GPMH600, GPMH650, GPMH700, and GPMH750, were used to measure the compressive strength after 7, 28, 90 and 180 days.

2.3 Physical properties

The compressive strength of the samples was measured with an Instron 1195 Compression machine with a displacement of 5 mm/min. The results shown are an average of five replicate cubic specimens. Dry density (ρ_d) was calculated according to European Standard EN 12390-7. Three samples (of each formulation) were oven dried at 105 °C for several days until stabilization of the mass. The total apparent volume V, dry density (ρ_d) and wet density (ρ_{water}) is then evaluated using following equations, (1) to (2), where M_d: mass dry; $M_{sat\ air}$: saturated mass in air (g); $M_{sat\ water}$:immersed saturated mass in water (g);

$$V = \frac{M_{sat\ air} - M_{sat\ water}}{\rho_{water}} \quad (1) \qquad \rho_d = \frac{M_d}{V} \quad (2)$$

2.4 Physico-chemical characterization methods

The specific surface areas of halloysite clay heated at 600, 650, 700 and 750 °C were determined according to Brunauer–Emmet–Teller (B.E.T.) method based on nitrogen adsorption using a Micromeritics GEMINI 2360 instrument. The particle size distributions (cumulative and density distribution) were investigated by means of a Mastersizer 2000 Ver. 5.22 (Malvern Instruments Ltd). Simultaneous Differential Thermal Analysis-Thermogravimetric analysis (DTA/TG) was performed on the four calcined halloysite and geopolymer samples, using a Netzsch STA 429 CD in air atmosphere. The analyses were carried out on ground powders (sieved below 80 µm) at a heating rate of 20 K/min in platinum-rhodium crucibles using calcined alumina as a reference. Meta-halloysite, and

172 geopolymer specimens aged for 28 days were crushed and sieved through a sieve of mesh 80
173 µm. The obtained powders were subjected to X-ray powder diffractometry (XRD; applying a
174 PW3710, Phillips) using CuKα, and Ni-filtered radiation (the wavelength was 1.54184 Å).
175 The radiation was generated at 40 mA and 40 kV. Each analysis was performed on fine grains
176 of ground samples. Random powder specimens were step-scanned from 5° to 70°, 2θ range,
177 and integrated at the rate of 2s per step. Pieces collected from the mechanical testing were
178 polished, gold coated for microstructural observations using a JEOL JSM-6500F Scanning
179 Electron Microscope (SEM) coupled with Energy Dispersive X-ray spectroscopy (EDX) with
180 an acceleration voltage of 10.0 kV. The apparatus was equipped with high resolution W
181 filament gun (LaB6 option). An integrated camera allowed intuitive navigation to the area of
182 interest of different samples. The initial setting time was measured on the fresh geopolymer
183 pastes obtained from calcined halloysite clay (600 and 750 °C), with alkaline solution using
184 Vicat apparatus. The needle used was 1.000 ± 0.005 mm in diameter. The initial setting is
185 verified from 10 min after the preparation of geopolymer pastes every minute until the first
186 resistance is detected. This was done in the laboratory with 60% of relative humidity and the
187 room temperature was 17 ± 2°C. This test was performed according to the EN196-3 standard.
188 The rheology of the geopolymer pastes was characterized using a stress-controlled rheometer-
189 ARG2 from TA Instruments. The measuring geometry consisted of a 25 mm upper and lower
190 plate temperature regulated with a Peltier. The viscoelastic parameters of fresh paste were
191 investigated by simple shear flow and dynamic oscillatory tests carried out at 21°C in the
192 linear viscoelastic domain. The geopolymer pastes were prepared by hand mixing outside the
193 rheometer and then introduced into the rheometer between the plates. Rheological steady state
194 flow measurements consisted in performing a series of creep experiments with varying stress,
195 where the equilibrium shear rate is obtained when the curve reaches a linear regime. The
196 linear viscoelastic region (LVER) was determined by oscillatory strain sweep from 0.002% to

20% at a fixed frequency of 1 Hz. Herschel-Bulkley law (equation 3) has been used to determine the viscoelastic parameters:

$$\tau = \tau_o + K\gamma^n \quad (3)$$

where τ_o is the yield stress, K the consistency and n the rate index. Viscoelastic properties of the geopolymer binders were investigated by oscillatory measurements. The basis of these measurements is the application of a sinusoidal strain (γ) and the measurement of the corresponding stress (τ). The loss modulus ($\tan\delta$) defined by $\tan\delta = \frac{G''}{G'}$ (4) was also analyzed during the geopolymerization. Isothermal (heat conduction) calorimetry was used to study the steps related to the geopolymerization of cement pastes at 27 °C on the early age (48h). The rate of heat evolution during the reaction (dq/dt) was evaluated using an eight-channel isothermal conduction calorimeter (TAM AIR, Thermometric AB, Jarafalla, Sweden). The main steps of the sample preparation were: the preparation of the alkaline activator solution, followed by the mixing of the alkaline activator with the powder sample and loading of the mixture in calorimeter. 7g of each calcined halloysite powder and the ratio of liquid/solid was 0.83 according to our previous work (Kaze et al.2018) for all the samples. The time-dependent degree of reaction $\alpha(t)$ was determined with the calorimetry data following the Stutter method, according to Equation 5:

$$\alpha(t) = Q_{(t)}/Q_{max} \quad (5)$$

Where $Q_{(t)}$ is the cumulative heat, released at time t, and $Q_{max}$is the total or the maximum heat released hear after 48h.

3. Results

3.1 Characterization of raw materials

219 The effect of thermal activation on granulometry of calcined halloysite clay at 600,
220 650, 700 and 750°C is depicted in Figure 1. No significant change in particles size of $d_{0.1}$ and
221 $d_{0.5}$ is observed with increasing of calcination temperature from 600 to 750 °C. However, a
222 slight increase of particle size was noted on $d_{0.9}$ (Table 1) from 42 to 58 µm. This trend could
223 be explained by the beginning agglomeration or sticking of particles due to the increase of the
224 calcination temperature from 700 to 750 °C. In all calcined halloysite samples labelled
225 MH600, MH650, MH700 and MH750, the particle size distribution is characterized by a
226 multimodal distribution. The first mode varies from 0.1 to 1µm with a maximum around a
227 size of 0.34 µm. In the second mode, particles range from 1 to 19 µm with a maximum around
228 5.7 µm. Finally, the last mode, situated between 19 and 183 µm has a maximum around 58
229 µm. Figure 2 presents the SEM images of raw halloysite clay (HA) and calcined halloysite
230 (MH700) at 700 °C. This was carried out at higher magnification to show in detail the
231 morphological shapes of halloysite clay before and after calcination (700 °C). The particles of
232 raw halloysite clay have platelet shapes, thus not similar to nanotubes as observed with TEM
233 by others (Yuan et al. 2008; Yuan et al. 2012; Li et al. 2019; Zhang et al. 2020). If the
234 halloysite is heated at 700 °C, the meta-halloysite exhibited spherical form and fine particles
235 consistent with the findings of Tchakoute et al. (2020). Heating halloysite clay from 600 to
236 750 °C changed their crystalline structure by transforming into amorphous phases attributed
237 to the dehydroxylation indicated on TG/DTA analyses. The fine particles observed on heated
238 samples would be beneficial during the geopolymerization reaction, because the fine particles
239 have a large surface area and could more rapidly dissolve in an alkaline solution. No diffusion
240 control is expected either, thus the particles can completely react. Hence with this kind of
241 particles one can expect a completely reacted solid phase, with a dense microstructure and
242 good mechanical properties of the end products. X-ray patterns of calcined halloysite clay
243 from 600 to 750 °C are reported in Figure 3. From Figure 3 one can observe the

disappearance of the halloysite mineral reflection from 650°C to 750°C indicating the total transformation or dehydroxylation of halloysite clay to meta-halloysite. The mineralogical phases were (Q) (SiO_2, PDF #5-349); hematite (He) (Fe_2O_3, PDF #13-5), except halloysite (H) ($Al_2Si_2O_5(OH)$, PDF #13-375) that was still present in calcined halloysite at 600 °C. On the other hand the X-ray diffractograms of all calcined halloysite clays labelled MH600, MH650, MH700 and MH750 showed a diffuse halo peak with 2θ ranging between 15° and 35° which is known as characteristic of amorphous and thus reactive phase present in calcined halloysite clays. This halo confirms the conversion of halloysite clay to meta-halloysite after calcination. Figure 4A highlights the simultaneous DTA/TG thermogram of raw halloysite clay. The thermogram shows two endothermic phenomena. The first, about 2 wt% is situated around 82 °C and corresponds to elimination of water. The second one, 11 wt%, centered at 542 °C, is attributed to the dehydroxylation of halloysite (Yuan et al. 2015). The exothermic phenomenon at about 997 °C corresponds to the transformation of meta-halloysite into mullite (Yuan et al. 2015). With the simultaneous differential thermal and thermogravimetric analysis (TG/DTA) carried out on calcined halloysite, it was possible to observe the major transformations which take place between 50 and around 500 °C (Figure 4B). The first endothermic situated around 50 °C is related to the loss of the non-structural water (Figure 4B). The second one at 465 °C on MH600 curve corresponds to loss of water of Al-OH groups of residual halloysite that did not totally transform to meta-halloysite when the halloysite clay was calcined at 600 °C (Figure 4B) (Yuan et al. 2015). This demonstrates that halloysite clay should be calcined above 600 °C as reported by the findings of Yuan et al. (2012) and Zhang et al. (2020), who reported that the halloysite crystals were completely destroyed and an amorphous phase formed between 650 and 850 °C. It is also noticed that the thermal treatment at 650, 700 and 750 °C does not change the thermograms of halloysite clay a lot. This observation can be confirmed with Figure 4C): at 650, 700 and 750 °C the mass

loss is within 2 wt% mainly due to absorbed water after the dehydration, and a small residual dehydroxylation step, starting each time at a higher temperature. The endotherm (in DTA curve) that appeared at 573 °C is linked to the transformation of α-quartz to β-quartz (van Riessen and Wall 2010). The last one around 980 °C is due to the formation of mullite phase (Yuan et al. 2015; Li et al. 2019; Tiffo et al. 2020; Youmoue et al. 2020) (Figure 4B). The infrared spectra of raw halloysite (HA) and calcined halloysite labelled MH600, MH650, MH700 and MH750 are plotted in Figure 5. For the raw halloysite clay (Figure 5A), the absorption bands located at 3619 and 3694 cm^{-1} are attributed to O-H stretching linked to halloysite mineral and axial asymmetric and symmetric deformation of Al-OH (Kaze et al. 2018a). Those situated at 910, 998 and 1118 cm^{-1} are assigned to the stretching vibration modes of Si-O-Si and Si-O-Al bonds (Figure 5A). The last bands at about 750-788 cm^{-1} and 676 cm^{-1} are linked to the distorted Al(VI) of octahedra of halloysite structure and vibration mode of Si-O bond, respectively (Kaze et al.2018; Tchakoute et al. 2020). The broad absorption bands at interval 1043-1053 cm^{-1} (Figure 5B) are assigned to internal vibration of Si-O-Si and Si-O-Al bindings (Lemougna *et al.* 2014; Baenla et al.2020). The ones located between 773 and 784 cm^{-1} correspond to the Al-O bending mode of AlO_6 (Muayad *et al.* 2015) octahedra in halloysite and meta-halloysite respectively in all samples (Figure 5B). The intensity of these bands decreases with thermal activation from 600 to 750°C, indicating the breakdown of the octahedral Al structure of the halloysite particles (Bich *et al.* 2009). The absorption bands at 663, 676, 678 and 692 cm^{-1} are attributed to the stretching of Si-O of quartz (Tchakoute *et al.* 2015; Kamseu et al. 2020). The last absorption bands situated in the range of 436-447 cm^{-1} correspond to Si-O-T(Al or Si) stretching and deformation vibration (Joussein *et al*. 2005; Nicolini *et al*. 2009).

3.2 Reactivity study

The different reaction steps during the first 48 h of geopolymerization reaction are shown in Figure 6A. According to this figure, three major peaks of heat evolution were detected during the first 48 h of geopolymerization reaction. The first step (I) appearing almost immediately on calorimetric curves when each calcined halloysite powder was mixed with alkaline solution, represents the dissolution of the glassy or amorphous phase contained in solid precursors. While the second peak (II) which is more distinct in all samples used for the calorimetry study depicts reorganization, diffusion of dissolved ions with formation of small, coagulated structures via condensation to build up an aluminosilicate gel phase. The third step (III) is the polycondensation thus the formation of the solid state due to the agglomeration of oligomer species corresponding to the hardening of geopolymer pastes using the Vicat test. The aforementioned phenomena (I) and (II) increase with the rise of calcination temperature. However, the increase is prominent from 600 to 700 ^{o}C and less from 700 to 750 ^{o}C. The reaction (II) reaches its maximum rate during ~ 4h in all the samples. The degree of reaction (α) (determined according to the equation 6 in section 2.4) at this maximum is 0.34, 0.37, 0.4 and 0.41 for MH 600, 650, 700 and 750 ^{o}C, respectively. The increase of calcination temperature from 600 to 700 ^{o}C considerably improved the reactivity of halloysite clay by the transformation of crystalline aluminosilicate (halloysite) to amorphous aluminosilicate (meta-halloysite). However, every material has the limit of the activation temperature. Up to this limit the contrary effect can be observed. Notice that from 700 to 750 ^{o}C the variation of energy and the reactivity is low. Based on calorimetry it is not necessary to activate the halloysite above 700 ^{o}C as the thermogram for 750 °C is the same within the margin of uncertainty. The shape of the heat released curves during these reactions is depicted in Figure 6B. The total heat released recorded on different calcined powders activated with alkaline solution after 48 h of reaction (obtained by integrating the heat flow according to the time) is 237, 241, 257 and 259 J/g for MH600, 650, 700 and 750°C, respectively. This heat released

318 drastically increased from 600 to 700 °C, but is almost the same at 700 or 750 °C. The heat
319 released is typical of exothermic reaction. The progress of heat released corroborates with the
320 above observations. The results of initial setting time as a function of the calcination
321 temperature of the meta-halloysite based geopolymer pastes from the calcined halloysite clays
322 between 600 and 750 °C using Vicat needle are reported in Table 2. It is observed that the
323 setting time varies between 326 and 196 minutes: it decreases when thermal activation is
324 carried out from 600 to 700 °C for GPMH600, GPMH650 and GPMH700 geopolymer
325 samples. This decrease is due to the increase in reactive fraction, but also in reactivity. The
326 link between these two is not so obvious as the reaction is heterogenous, thus the first step of
327 the reaction takes place at the interface between solid and liquid. It is clear from ICC (Figure
328 6A, inset) that also the first step (dissolution) is faster, finally leading to an overall faster
329 reaction. The available reactive phases that allowed the decrease of setting time might be
330 explained by the almost total transformation of halloysite clay to meta-halloysite which can
331 provide more reactive silicates and aluminates. Above 700 °C, a small increase is noticed till
332 210 minutes for geopolymer labelled GPMH750. This increase was not expected based on the
333 calorimetry results where MH750 is not slower than MH700. This small increase in setting
334 time might be due to the further rearrangements in the meta-halloysite, which decreased the
335 solubility again. This will lead to a lower availability of Al-species in alkaline medium
336 required to polymerize or polycondensate with Si-species during the geopolymerization
337 reaction. To further clarify the exact reasons for this slow down, extra investigations are
338 needed such as Nuclear Magnetic Resonance (NMR) spectroscopy to investigate the
339 surroundings of ^{29}Si and ^{27}Al in the meta-halloysite and in the geopolymer binder, but this is
340 not the main target of this research. A similar trend was observed by Elimbi *et al*. (2011) on
341 the effect of calcination temperature on the reactivity of metakaolin based geopolymer. These

342 authors concluded that the increase in setting on samples heated above 700 °C is linked to the
343 decrease of reactive or amorphous phase necessary for geopolymer synthesis.

344 3.3 Rheological behaviour

345 Figure 7 depicts the oscillatory strain sweep of meta-halloysite geopolymer pastes at 1
346 Hz. In all geopolymer formulations, namely: GPMH600 (Figure. 7A), GPMH650 (Figure.
347 7B), GPMH700 (Figure. 7C) and GPMH750 (Figure. 7D), the elastic modulus (G') is higher
348 than the viscous modulus (G'') in the linear viscoelastic region (LVER) describing the gel-
349 like behaviour. The LVER is the region where G' and G" do not change with the amplitude.
350 This region is below a strain of 0.01% in all cases. In this region the interaction between
351 different constituents is related to predominance of geopolymer gel (N-A-S-H) network
352 formation even before hardening of different sample pastes (Poulesquen *et al*. 2013). Similar
353 trend was observed by Martin *et al.* (2018) and Poulesquen et al. (2011) on rheological
354 properties of alkali-activated brick powder-based pastes and metakaolin based geopolymer
355 using different activators, respectively. These authors concluded that the solid properties of
356 alkali activated materials are linked to first step (dissolution of solid precursor into oligomers
357 formation) and second step (polycondensation of oligomers into rigid block) of
358 geopolymerization mechanism. These observations are in agreement with the ICC study. At
359 the crossover point where G'=G'', G'' quickly exceeds the elastic modulus in all geopolymer
360 samples GPMH600, GPMH650, GPMH700 and GPMH750, indicating the consistency of a
361 rigid amorphous solid 3-D geopolymer network resulting from polycondensation of silicate
362 and aluminate oligomers during the geopolymerization reaction (Palacios *et al.* 2018; Puertas
363 *et al.* 2018; Rovnaník *et al.* 2018). At this point the strain decreases from 0.23% to 0.08 %
364 with calcination temperature from 600 to 700 °C. This trend could be justified by the increase
365 of reactive or amorphous fraction within calcined halloysite clay. A slightly increase in strain
366 noticed on GPMH750 (0.14%) confirms the aforementioned reduction of reactive phase. The

367 values of yield stress of specimens were obtained using the Herschel-Bulkley model fitted to
368 the data. The values were 5.43, 3.70, 2.50 and 5.54 Pa for GPMH600, GPMH650, GPMH700
369 and GPMH750 samples, respectively. As seen in Figure 7, the yield stresses decrease from
370 5.43 Pa (GPMH600) to 2.45 (GPMH700) indicating the increase of reactive phase within
371 calcined halloysite resulting in fast setting in contact of alkaline solution, and increased from
372 2.45 to 5.54 Pa (GPMH750) related to the formation of coarse particles after calcination at
373 700 °C leading to high interactions in alkaline medium linking to low reactivity. When G'' '
374 pass over G' at gel point, the loss modulus (Tanδ) increased in samples and reached a peak at
375 12 % of strain then decreased (Figures 7a-d). This corresponds to the gradual gelation of
376 geopolymer microstructure pastes (Rovnaník *et al.* 2018). Figure 8A presents the evolution of
377 compliance of geopolymer formulations as function as time. It is shown that the deformations
378 (compliances) undergone by GPMH600, GPMH650, GPMH700 and GPMH750 geopolymer
379 pastes decrease with increasing of calcination temperature from 600 to 750 °C. The increase
380 in deformation is characteristic of high interaction between different phases in geopolymer
381 GPMH650, GPMH700 and GPMH750 pastes related to the important amount of reactive
382 phase compared to lower compliances undergone by geopolymer GPMH600 paste where the
383 interparticle bonds are weak. In all curves it is noted that the compliance increases, reaches
384 the maximum and remain almost constant with time indicating the hardening of geopolymer
385 paste. For the all formulations a residual strain in pastes was observed. The values were 0.02,
386 0.15, 0.07 and 0.10 Pa^{-1}, respectively for GPMH600, GPMH650, GPMH700 and GPMH750.
387 These values were achieved at 1393, 1116, 1065 and 1015s, respectively. Thus, the increase
388 in calcination temperature improved the meta-halloysite based geopolymer pastes rheological
389 behaviour resulting in competition between dissolution of amorphous phase and
390 geopolymerization process that could affect the rheology evolution of the elaborated

391 geopolymers. This trend is in line with the setting time results and ICC analysis. These results
392 confirm those obtained from the oscillatory tests.

393 3.4 Phases evolution

394 Figure 8B displays the infrared spectra of meta-halloysite based geopolymer
395 GPMH600, GPMH650, GPMH700 and GPMH750 samples. The broad absorption bands that
396 appears in the range of 1618-1634 cm^{-1} and 3379-3419 cm^{-1} correspond to the stretching and
397 deformation vibration modes of H-O-H and O-H of water molecules. The bands that appear at
398 1043-1053 cm^{-1} in the meta-halloysite IR spectrum after activated with alkaline solution
399 shifted toward lower wavenumbers 973, 976, 979 and 990 cm^{-1} for GPMH600, GPMH650,
400 GPMH700 and GPMH750, respectively. This displacement indicates the change of structure
401 that occurred during depolymerization and polycondensation process resulting in
402 incorporation of Al tetrahedra into silicate footprint (Rahier *et al.* 1997; Balo *et al.* 2018). On
403 the other hand these absorption bands are attributed to the asymmetric stretching of Si-O-Al
404 bonds in geopolymer network, known as characteristic peak of inorganic polymer network in
405 literature (Aldabsheh *et al.* 2015; Rees *et al.* 2007; Peys *et al.*2016). The small bands at 774-
406 775 cm^{-1} are linked to Al-O bending. The bands situated at 670-699 cm^{-1} and 415-431 cm^{-1}
407 are assigned to asymmetrical and symmetrical stretching vibration modes of bridge bonds of
408 Si-O-Si, Si-O-Al and Si-O bonds respectively (Kaze et al. 2017; Nana *et al.* 2019). The
409 thermal analysis performed on different consolidated meta-halloysite based geopolymer
410 binders are shown in Figures 8C-D. From the DTA curves (Figure 8C) the endothermic peaks
411 in all geopolymer samples at 50 °C accompanied with 2.0 and 4.0% of weight loss on TG
412 curves (Figure 8D), are linked to the evaporation of free water (Alomayri *et al.* 2014; Assaedi
413 et al. 2020). While the second one centred about 105 °C which accounted for about 70% of
414 the total weight loss in 25-1200 °C in all meta-halloysite thermograms is assigned to the
415 release of water chemically or physically bounded to Na-aluminosilicate binder phase within

geopolymer matrix resulting in denaturation or break down of geopolymer network (Rashad and Ouda 2018). The exothermic peaks located at 875 and 954 °C (Figure 8C) imply the reorganization of non-reactive meta-halloysite particles in alkaline medium which allowed the formation of mullite phase (Lecomte-nana *et al.* 2012; Deutou et al. 2020). These peaks are more noticeable in the TG/DTA curves of calcined halloysite at different temperatures (600, 650, 700 and 750 °C) compared to those of meta-halloysite based geopolymer binders (GPMH700 and GPMH750) which are less significant. This indicates that a major part of alumina particles from meta-halloysite had reacted with sodium activating solution to form sodium-alumino-silico-hydrated (N-A-S-H) binder and less amorphous or semi-crystalline aluminium compounds. The X-ray patterns of meta-halloysite based geopolymer binders are reported in Figure 9. It is observed the disappearance of residual halloysite presents in calcined halloysite at 600 °C after alkaline activation. This could be due to their dissolution resulting into zeolite in alkaline medium. However, the main minerals like hematite, anatase and quartz present in all calcined halloysite (from 600 to 750 °C) are still present after geopolymerization reaction, suggesting that these minerals had not altered in alkaline medium thus would behave as micro aggregates or fillers by reinforcing the geopolymer matrix. The displacement of broad hump situated between 2θ = 15° and 35° (Figure 3) in calcined halloysite clay at different temperatures to 20° and 40° (Figure 9) for all meta-halloysite based geopolymers, indicates the formation of amorphous binder (Na-aluminosilicate) phase responsible to the strength development gained on samples mechanically tested. The intensity of amorphous phase increases with thermal activation from 600 to 750 °C is in agreement with the reactive degree observed by kinetic reaction analysis.

3.5 Mechanical and physical properties

The compressive strengths of hardened geopolymer binders as a function of the thermal activation of the halloysite clay were reported in Table 2. As can see from this Table

441 (Table 2) the mechanical performance increases from 600 to 700 °C then drops afterward.
442 The compressive strengths of hardened meta-halloysite-based geopolymer specimens were
443 18.30/28.82/31.30/32.30MPa; 28.90/58.40/62.40/66.80MPa; 29.90/61.50/65.50/68.70MPa;
444 30.23/68.50/70.34/73.70MPa respectively for geopolymer binders made from calcined
445 halloysite clay (at 600, 650, 700 and 750 °C) cured at 7, 28, 90 and 180 days. However, no
446 large change in strength development was noticed between the samples made from calcined
447 halloysite between 700 and 750 °C. The increase of compressive strength of meta-halloysite
448 based geopolymers made from calcined halloysite clay from 600 to 750 °C is justified by the
449 increase of reactive phase within calcined powders which can easily dissolve into alkaline
450 solution by producing an extend geopolymer network resulting in a compact structure. It is
451 obvious that the increase in thermal activation from 600 to 750 °C improves the amorphous
452 phase content (within meta-halloysite) leading to better mechanical performances of
453 geopolymer specimens. It is noteworthy that the obtained fine particles from calcined
454 halloysite played an important role during the geopolymerization reaction contributing to a
455 high dissolution of solid precursor resulting in high degree of polymerization or
456 polycondensation between Al- and Si- oligomer species. This favours the cohesion and
457 bonding strength between different particles in geopolymer matrix suggesting a compact end
458 product. The increase in compressive strength of meta-halloysite based geopolymer with
459 calcination temperature from 600 to 750 °C is consistent with observation Zhang et al. (2020)
460 who found that 750 °C is the optimal temperature to ensure a high strength (58.7 MPa) from
461 calcined halloysite clay favourable for geopolymerization. However, calcination above 700
462 °C does not remarkably improve the strength development even though the compressive
463 strength achieved on samples made of MH750 is still high. Only at longer times, the MH750
464 based samples have still significant higher strengths. This trend might be related either to less
465 available Al for polycondensation or decrease of the amorphous phase content, resulting to

466 less performant strength between geopolymer products GPMH700 and GPMH750 cured at 7,
467 28, 90 and 180 days. Only 2, 7 and 5 MPa gained in compressive strength from GPMH700 to
468 GPMH750 samples cured at 28, 90 and 180 days. This result is in line with the one of kinetic
469 reaction explained earlier (section 3.2) where low total heat (about 2.20 J/g) was recorded
470 between GMH700 and GPMH750 samples even this later had more total heat released than
471 GPMH600, GPMH650 and GPMH700 specimens suggesting higher reaction degree. The
472 bulk density of meta-halloysite based geopolymers is reported in Table 2. The density ranges
473 from 1.98 to 1.67 g/cm^3; 1.97 to 1.86 g/cm^3; 1.96 to 1.88 g/cm^3; 1.95 to 1.86 g/cm^3, for
474 specimens GPMH600, GPMH650, GPMH700 and GPMH750, respectively. As listed in
475 Table 2 it is noticed that the bulk density decreases considerably from 7 to 90 days for
476 GPMH600 sample, and from 7 to 28 days for samples GPMH650, GPMH700 and GPMH750,
477 and then becomes almost constant from 28 to 180 days. The high decrease of bulk density
478 observed on GPMH600 sample can be justified by either the loss of the extra water that has
479 not taken part in geopolymerization or water evaporation during the drying which makes the
480 sample lighter with time. This also proves that the thermal activation at 600 °C does not
481 produce a sufficient amount of reactive phase available for the well geopolymerization
482 process. This behaviour is in agreement with the one of Djobo *et al.* 2016, who attributed the
483 decrease of bulk density to the increase of apparent porosity. Table 2 also shows the evolution
484 of the amount of absorbed water in the function of curing time. The water absorption varies
485 from 18% to 24%; 15% to 19%; 12% to 17% and 12% to 16%, for specimens labelled
486 GPMH600, GPMH650, GPMH700 and GPMH750, respectively. The maximum water
487 absorption was recorded between 7 and 28 days while after 90 days, it is no significant
488 variation and remains almost constant with curing time where these values decreased and
489 ranged from 24% to 18%; 19% to 13%; 17% to 9% and 16% to 10%, respectively for
490 geopolymers GPMH600, GPMH650, GPMH700 and GPMH750. The high values of water

491 absorption observed on samples GPMH600 are attributed to the presence of residual
492 halloysite clay within calcined halloysite at 600 °C, which can retain much water when the
493 specimens were immersed in water for the water absorption test.

494 3.6 Scanning electron microscope (SEM)

495 Figure 10 presents the selected fractures of SEM micrographs detailing the internal
496 microstructure of meta-halloysite based geopolymer binders made from calcined halloysite
497 clay between 600 and 750 °C. The geopolymer matrix appears to exhibit an inhomogeneous
498 structure. In Figure 10A, it is observed a typical semi-spherical pore on the fractured surface,
499 surrounded by geopolymer matrix with microcracks on geopolymer sample GPMH600, while
500 the GPMH650, GPMH700 and GPMH750 specimens are more compact. These pores are
501 likely caused by the air bubbles that are introduced into the geopolymer pastes through
502 mixing or trapped inside the geopolymer binder when pouring into moulds. On the other
503 hand, the presence of microcracks might be obviously formed after mechanical testing where
504 collected pieces were used for SEM analysis. Therefore, the less dense and compact sample
505 would be more affected by exhibiting more fissure after mechanical testing measurements, it
506 is the case of MH600 sample compared to other specimens. This proves the lower reactivity
507 and mechanical strength gained on sample labelled GPMH600 obtained from calcined
508 halloysite at 600 °C. At higher magnification images (≤ 1µm), it is also observed that the
509 GPMH600 specimen contains a greater quantity of microspheres than GPMH650, GPMH700
510 and GPMH750 samples, while the opposite was observed for platy films belonging to non-
511 reactive meta-halloysite powders (Figure 10B). It is believed that the platy films appearing on
512 microstructure, are geopolymer binders which embed other particles as unreactive phases
513 within matrix. The increase of the thermal activation from 600 to 750 °C leads to
514 enhancement of reactive phase (amorphous) in calcined halloysite, which release more
515 reactive silica and alumina in contact of alkaline solution during the dissolution step, resulting

516 in good polycondensation allowing a very compact and dense structure justifying the high
517 strength gained in this study. This trend is in agreement with the work done by Davidovits *et*
518 *al.* (1988); Palomo *et al.* (1999), and Cioffi *et al.* (2003), conducted on calcined kaolinite clay
519 in the range of 550-800 °C. These authors stated that the increase of calcination temperature
520 improves the compressive strength resulting in compactness of metakaolin based
521 geopolymers. Similar trend was recently noticed by Zhang et al. (2020) on thermally
522 halloysite clay used as solid precursor for geopolymer synthesis.

523 **4 Discussion**

524 Halloysite clay belongs to 1/1 clay type as kaolinite. It contains majority of silicon and
525 aluminium oxides which are fundamental ingredients of geopolymerization reaction
526 (Davidovits 2008) thus suitable for making inorganic polymers (geopolymers). The thermal
527 treatment of halloysite clay from 600 to 750 °C enhances the reactivity (amorphous phase) of
528 resulting meta-halloysite powder. This would favour a high dissolution of reactive phase
529 followed by polycondensation of Si- and Al-oligomers giving geopolymer binders with
530 optimum mechanical strength compared to that of metakaolin based geopolymers found in
531 literature (Selmani *et al.* 2017; Sun and Vollpracht 2018). From FTIR spectra the degree of
532 dehydroxylation (D_{IR}) was evaluated using a formula $D_{IR}=1-S/So$ (where S and So represent
533 peak area and maximum peak area respectively) as reported by Rahier *et al.* (2000). It was
534 found that the degree of dehydroxylation increases with the rise of calcination temperature.
535 These values ranged from 0.98 to 1. For the calcined halloysite MH650, MH700 and MH750
536 $D_{IR}=1$, indicating the total transformation of halloysite clay to reactive or amorphous meta-
537 halloysite at these temperatures. This result is in agreement with TG/DTA analysis carried
538 earlier on different calcined halloysite samples. In previous work carried on dehydroxylation
539 of kaolinite studied by Rahier *et al.* (2000), they showed that during the calcination of
540 kaolinite, the degree of dehydroxylation slightly increases from 550 to 700 °C and remained

almost constant and equal to 1 above 700 °C. Whereas in our case studied here from 650 to 750 °C the controversy effect was observed. This could be explained by the disposition or shape of minerals phase in halloysite which seem to reduce the calcination temperature ≤ 700 °C as compared to that of standard metakaolin based geopolymer. The final properties gained on meta-halloysite based in this research are in agreement with their fine particles compared to that of standard metakaolin which seem to well behave in alkaline solution. This finesse of particles might favour the high dissolution of solid precursor in alkaline medium resulting in an important geopolymer binder content required for the good cohesion between different components in the geopolymer matrix leading to compact and dense structure as previously reported by Kaze et *al*. (2020) and Tchakoute et *al*. (2020). As the compressive strength increased as well as thermal activation, the use of Nuclear Magnetic Resonance (NMR) spectroscopy needs to be conducted to assess the behaviour of Si and Al during the formation of geopolymer network at different calcination temperatures. The little increase in mechanical strength and setting time between GPMH700 and GPMH750 °C geopolymer samples would be assessed using NMR spectroscopy.

5 Conclusions

This study aimed to investigate the use of meta-halloysite powders from calcined halloysite clay from 600 to 750 °C in light to correlate the thermal activation with reactivity and the strength development. The following conclusions carry on meta-halloysite based geopolymers cured at room temperature can be drawn.

1. The increase of calcination temperature from 600 to 750 °C considerably improved the reactivity of halloysite clay by the increase of amount of amorphous phase within meta-halloysite.
2. From isothermal conduction calorimetry (ICC) it was observed that GPMH750 and GPMH700 had almost the more total heat released compared to that of GPMH600

GPMH650 samples indicating higher reaction degree. Thus, 750 °C appears here as the suitable temperature for the thermal activation of the halloysite clay to ensure high strength.

3. The mechanical properties of meta-halloysite based geopolymers remarkably increased with calcination temperature from 600 to 700 °C and slightly between 700 and 750 °C.
4. The microstructure of resultant geopolymer products GPMH650, GPMH700 and GPMH750 are more compact and denser compared to that of GPMH600. This trend is line with the increase in amount of reactive or amorphous phase responsible to higher polycondensation of geopolymer network resulting in high development strength.
5. Although a little increase in compressive strength and setting time between 700 and 750 °C, the utilization of 750 °C as calcination temperature would not be economical and sustainable for the geopolymer binder in high scale.

Apart from the above findings, further attention would be paid to measurement of NMR spectroscopy analysis for more details investigation to optimise the study.

6 Acknowledgments

RCK gratefully acknowledges Department of Physics, Umm Al-Qura University, Makkah 21955, Saudi Arabia for running characterization of the geopolymers products made in this research paper. The authors are grateful to Ingessil S.r.l., Verona, Italy, for providing sodium silicate used. Thankful would also be addressed to Mr Michaël LACROIX for his helping during the Rheological measurements at the University of Limoges during my internship.

7 References

Achile Nana, Jean Ngouné, Rodrigue C. Kaze, Likiby Boubakar, Serge K. Tchounang, Hervé K. Tchakouté, Elie Kamseu, Cristina Leonelli. 2019. Room-temperature alkaline

591 activation of feldspathic solid solutions: Development of high strength geopolymers.
592 *Construction and Building Materials* 195 (2019) 258–268.

593 Aldabsheh, Islam, Hani Khoury, Jan Wastiels, and Hubert Rahier. 2015. "Dissolution
594 Behavior of Jordanian Clay-Rich Materials in Alkaline Solutions for Alkali Activation
595 Purpose. Part I." *Applied Clay Science* 115: 238–47.

596 Alomayri, Thamer, Les Vickers, Faiz U A Shaikh, and It Meng Low. 2014. "Mechanical
597 Properties of Cotton Fabric Reinforced Geopolymer Composites at 200–1000 °C."
598 *Journal of Advanced Ceramics* 3 (3): 184–93.

599 Assaedi Hasan, Thamer Alomayri, Cyriaque Rodrigue Kaze, Bharat Bhushan Jindal, Subaer
600 Subaer, Faiz Shaikh, Shoroog Alraddadi. 2020. Characterization and properties of geopolymer
601 nanocomposites with different contents of nano-$CaCO_3$. Construction and Building Materials
602 252 (2020) 119137.

603 Baenla J., J.B. Bike Mbah, I.B. Djon Li Ndjock, A. Elimbi. 2020. Partial replacement of low
604 reactive volcanic ash by cassava peel ash in the synthesis of volcanic ash based
605 geopolymer. Construction and Building Materials 227 (2019) 116689.

606 Bakharev, T. 2006. "Thermal Behaviour of Geopolymers Prepared Using Class F Fly Ash and
607 Elevated Temperature Curing." *Cement and Concrete Research* 36 (6): 1134–47.

608 Balo A. Madi, H. Rahier, A. Mobili, A. Katsiki, N. Fagel, U. Melo Chinje, D.
609 Njopwouo.2018. Metakaolin-based inorganic polymer synthesis using cotton shell ash as sole
610 alkaline activator. Construction and Building Materials 191 (2018) 1011–1022.

611 Blaise Ngwem Bayiha, Ndigui Billong, Emmanuel Yamb, Rodrigue Cyriaque Kaze, Robert
612 Nzengwa.2019. Effect of limestone dosages on some properties of geopolymer from
613 thermally activated halloysite. *Construction and Building Materials* 217 (2019) 28–35.

614 Brachhold, Nora, and Christos G Aneziris. 2013. “Porous Materials for Alkali Contaminated
615 Environments.” *Journal of the European Ceramic Society*. Volume 33, Issue 10, September
616 2013, Pages 2013-2021

617 Bich Ch., Ambroise J., Péra J. 2009. Influence of degree of dehydroxylation on the pozzolanic
618 activity of metakaolin. *Applied Clay Science* 44 (2009) 194-200.

619 Cioffi R., Maffucci L., Santoro, Optimization of geopolymer synthesis by calcination and
620 polycondensation of a kaolinitic residue. 2003. Ressource, Conservation and Recycling 40
621 (2003) 27-38.

622 Davidovits, J. (2008) Geopolymer Chemistry and Applications. Geopolymer Institute, Saint-
623 Quentin.

624 Davidovits, Joseph. 2015. *Geopolymer Chemistry and Applications*. 4th ed.

625 Deutou Juvenal N.G., Van Essa L.S. Kamga, R.C. Kaze, E. Kamseu, Vincenzo M.
626 Sglavo.2020. Thermal behaviour and phases evolution during the sintering of porous
627 inorganic membranes. Journal of the European Ceramic Society Volume 40, Issue 5, May
628 2020, Pages 2151-2162. https://doi.org/10.1016/j.jeurceramsoc.2020.01.035.

629 Elimbi A., Tchakoute H. K., M Kondoh., J Dika Manga**.** 2011. Thermal behavior and
630 characteristics of fired geopolymers produced from local Cameroonian métakaolin. *Ceramics*
631 *International 40 (2014) 4515-4520.*

632 Gisèle L. Lecomte-Nana, Khaoula Lebdiou, Mylène Laffort, Nadia Hout, Nicolas Tessier-
633 Doyena, Younès Abouliatim, Claire Peyratout.2017. effect of phyllosilicate type on the
634 microstructure and properties of kaolin-based ceramic tapes. Developments in Strategic
635 Ceramic Materials II: A Collection of Papers Presented at the 40th International Conference
636 on Advanced Ceramics and Composites, Volume 37, Issue 7 Edited by Waltraud M. Kriven,

637 Jingyang Wang, Yanchun Zhou, Dongming Zhu and Gustavo Costa Copyright © 2017 by The
638 American Ceramic Society
639 Idumah Christopher Igwe, Azman Hassana, James Ogbu, J.U Ndem and Iheoma Chigoziri
640 Nwuzor.2018. Recently emerging advancements in halloysite nanotubes polymer
641 nanocomposites. Composite Interfaces, DOI: 10.1080/09276440.2018.1534475
642 Joussein E., S. Petit, J. Churchman, B. Theng, D. Righi AND B. Delvaux. 2005. Halloysite
643 clay minerals a review. Clay Minerals (2005)40, 383–426.

644 Kamseu, E., A. Rizzuti, C. Leonelli, and D. Perera. 2010. "Enhanced Thermal Stability in
645 K_2O-Metakaolin-Based Geopolymer Concretes by $Al_2O_3$and SiO_2fillers Addition."
646 *Journal of Materials Science* 45 (7): 1715–24.

647 Kamseu Elie, Cyriaque Rodrigue Kaze, Joelle Nadia Nouping Fekoua, Uphie Chinje Melo,
648 Sylvie Rossignol, Cristina Leonelli. 2020. Ferrisilicates formation during the
649 geopolymerization of natural Fe-rich aluminosilicate precursors. Materials chemisrty and
650 physics 240(2020) 122062.

651 Kaze Cyriaque Rodrigue, L.M. Beleuk à Moungam, M.L. Fonkwe Djouka, A. Nana,
652 E.Kamseu, U.F Chinje Melo, C. Leonelli. 2017. The corrosion of kaolinite by iron minerals
653 and the effects on geopolymerization. Applied Clay Science 138 (2017) 48–62.
654 Kaze, Cyriaque Rodrigue, Herve Kouamo Tchakoute, Theophile Tchakouteu Mbakop,
655 Jacques Richard Mache, Elie Kamseu, Uphie Chinje Melo, Cristina Leonelli, and Hubert
656 Rahier. 2018. "Synthesis and Properties of Inorganic Polymers (Geopolymers) Derived
657 from Cameroon-Meta-Halloysite." *Ceramics International* 44 (15): 18499–508.

658 Kaze Cyriaque Rodrigue, Paul Venyite, Achile Nana, Deutou Nemaleu Juvenal, Herve
659 Kouamo Tchakoute, Hubert Rahier, Elie Kamseu, Uphie Chinje Melo, Cristina Leonelli.
660 2020. Meta-halloysite to improve compactness in iron-rich laterite-based alkali activated

materials. Materials Chemistry and Physics (239) 122268.

Kenne, B B Diffo, A Elimbi, M Cyr, J Dika Manga, and H Kouamo Tchakoute. 2014. “Effect of the Rate of Calcination of Kaolin on the Properties of Metakaolin-Based J. Asian Ceram. Soc. 3 (1), 130–138. http://dx.doi.org/10.1016/j.jascer.2014.12.003.

Lázaro, Blanca Bauluz. 2015. Halloysite and kaolinite : two clay minerals with geological and technological importance. Rev. Real Academia de Ciencias. ISSN: 0370-3207. 70: 7–38.

Lecomte-nana, Gisèle, Jean-pierre Bonnet, and Nibambin Soro. 2012. “Influence of Iron onto the Structural Reorganization Process during the Sintering of Kaolins.” *Journal of the European Ceramic Society*.

Lemougna, Patrick N., U. F. Chinje Melo, Marie Paule Delplancke, and Hubert Rahier. 2013. “Influence of the Activating Solution Composition on the Stability and Thermo-Mechanical Properties of Inorganic Polymers (Geopolymers) from Volcanic Ash.” *Construction and Building Materials* 48: 278–86.

Lemougna, Patrick Ninla, Achille Balo Madi, Elie Kamseu, Uphie Chinje Melo, Marie Paule Delplancke, and Hubert Rahier. 2014. “Influence of the Processing Temperature on the Compressive Strength of Na Activated Lateritic Soil for Building Applications.” *Construction and Building Materials* 65: 60–66.

Leonelli, Cristina, Elie Kamseu, Isabella Lancellotti, and Luisa Barbieri. 2017. “Geopolymerization as Cold-Consolidation Techniques for Hazardous and Non-Hazardous Wastes. Key Engineering Materials. 751: 527–31. doi.10.4028/www.scientific.net/KEM.751.527

Li Xiaoguang, Ding Wang, Qinfu Liu, Sridhar Komarneni. 2019. A comparative study of synthetic tubular kaolinite nanoscrolls and natural halloysite nanotubes. Applied Clay

684 Science 168 (2019) 421–427.

685 Martin VYŠVAŘIL, ROVNANÍKOVÁ Pavla, KEPPERT Martin.2018. Rheological
686 Properties of Alkali-Activated Brick Powder Based Pastes: Effect of Alkali Activator and
687 Silicate Modulus. Solid State Phenomena ISSN: 1662-9779, Vol. 276, pp 185-191
688 doi:10.4028/www.scientific.net/SSP.276.185 © 2018 Trans Tech Publications, Switzerland.

689 M.R. Wang, D.C. Jia, P.G. He, Y. Zhou. 2010. Influence of calcination temperature of kaolin
690 on the structure and properties of final geopolymer. Materials Letters 64 (2010) 2551–2554.

691 Muayad, Esaifan, Rahier Hubert, Barhoum Ahmed, Khoury Hani, and Hourani Mohammed.
692 2015. Development of Inorganic Polymer by Alkali-Activation of Untreated Kaolinitic
693 Clay : Reaction Stoichiometry , Strength and Dimensional Stability. Construction and
694 Building Materials 91 (2015) 251–259

695 Nicolini Keller Paulo, Cristiane Regina Budziak Fukamachi, Fernando Wypych, Antonio
696 Salvio Mangrich.2009. Dehydrated halloysite intercalated mechanochemically with urea:
697 Thermal behavior and structural aspects. Journal of Colloid and Interface Science 338 (2009)
698 474–479.

699 Palacios M., M.M. Alonso, C. Varga, F. Puertas.2018. Influence of the alkaline solution and
700 temperature on the rheology and reactivity of alkali-activated fly ash pastes. Cement and
701 Concrete Composites (2018), doi: 10.1016/j.cemconcomp.2018.08.010.

702 Palomo A., Blanco-Varela M.T., Granizo M.L., Puertas F., Vazquez T., Grutzeck M.W.
703 Chemical stability of cementitious materials based on metakaolin. Cement and Concrete
704 Research 29 (1999a) 997-1004.

705 Pemunta N.V., 2014.The ‘gendered field’ of kaolinite clay production performance
706 characteristics among the Balengou, Social. Anal. 58 (2) (2014) 21–41,

707 Peys, Arne, Hubert Rahier, and Yiannis Pontikes. 2016. "Applied Clay Science Potassium-
708 Rich Biomass Ashes as Activators in Metakaolin-Based Inorganic Polymers." Applied
709 Clay Science 119: 401–9.

710 Poulesquen A., F. Frizon, and D. Lambertin.2013. Chapter 20 Rheological Behavior of
711 Alkali-Activated Metakaolin During Geopolymerization. F. Bart et al. (eds.), Cement-Based
712 Materials for Nuclear Waste Storage, DOI 10.1007/978-1-4614-3445-0_20, # Springer
713 Science+Business Media New York 2013.

714 Provis, John L, and Susan A Bernal. 2014. Geopolymers and Related Alkali-Activated
715 Materials. Annu. Rev. Mater. Res. 2014. 44:3.1–3.29.

716 Puertas F., M.M: Alonso, S. Gismera, M. Lanzón and M.T. Blanco-Varela.2018. Rheology of
717 Cementitious Materials: Alkali-Activated Materials or Geopolymers. MATEC Web of
718 Conferences 149, 01002 (2018) CMSS-2017.

719 Rahier H., B. Wullaert, B. Van Mele, Influence of the degree of dehydroxylation of kaolinite
720 on the properties of aluminosilicate glasses. 2000. J. Therm. Anal. Calorim. 62 (2000)
721 417–427.

722 Rahier, H, Simons, W, VanMele, Biesemans, M. Low-temperature synthesized
723 aluminosilicate glasses.1997. Influence of the composition of the silicate solution on
724 production, structure and properties journal of materials science, 32 (1997) pages 2237–
725 2247.

726 Rashad, Alaa M., and Ahmed S. Ouda. 2018. "Thermal Resistance of Alkali-Activated
727 Metakaolin Pastes Containing Nano-Silica Particles." Journal of Thermal Analysis and
728 Calorimetry. 136 (2019) pages 609–620. https://doi.org/10.1007/s10973-018-7657-1

729 Rees, Catherine A, John L Provis, Grant C Lukey, and Jannie S J Van Deventer. 2007. "In

730 Situ ATR-FTIR Study of the Early Stages of Fly Ash Geopolymer Gel Formation," no.
731 18: 9076–82.

732 Rovnaník Pavel, Pavla Rovnaníková, Martin Vyšvarˇil, Stefania Grzeszczyk ,El_zbieta
733 Janowska Renkas.2018. Rheological properties and microstructure of binary waste red brick
734 powder/metakaolin geopolymer. Construction and Building Materials 188 (2018) 924–933

735 Selmani, Samira, Ali Sdiri, Samir Bouaziz, and Sylvie Rossignol. 2017. "Geopolymers Based
736 on Calcined Tunisian Clays: Effects of Alkaline Solution on Vibrational Spectra and
737 Mechanical Properties." International Journal of Mineral Processing 165: 50–57.

738 Sun, Zengqing, and Anya Vollpracht. 2018. "Isothermal Calorimetry and In-Situ XRD Study
739 of the NaOH Activated Fly Ash, Metakaolin and Slag." *Cement and Concrete Research*
740 103 (November 2017): 110–22.

741 Tchakoute, H. K., C. H. Rüscher, J. N.Y. Djobo, B. B.D. Kenne, and D. Njopwouo. 2015.
742 "Influence of Gibbsite and Quartz in Kaolin on the Properties of Metakaolin-Based
743 Geopolymer Cements." Applied Clay Science 107: 188–94.

744 Tchakoute Hervé Kouamo, Sorelle Joallita Kengne Melele, Aubin Tchandji Djamen,
745 Cyriaque Rodrigue Kaze, Elie Kamseu, Charles P. Njiki Nanseu, Cristina Leonelli, Claus
746 Henning Rüscher. 2020. Microstructural and mechanical properties of poly(sialate-
747 siloxo) networks obtained using metakaolins from kaolin and halloysite as
748 aluminosilicate sources: A comparative study. Applied Clay Science 186 (2020) 105448.

749 Tiffo Emmanuel, Jean Batiste Bike Mbah, Placide Désiré Belibi Belibi, Jean Noel Yankwa
750 Djobo, Antoine Elimbi. 2020. Physical and mechanical properties of unheated and
751 heated kaolin based-geopolymers with partial replacement of aluminium hydroxide.
752 Materials Chemistry and Physics 239 (2020) 122103.

753 Tome, Sylvain, Marie-Annie Etoh, Jacques Etame, and Kumar Sanjay. 2019. “Improved
754 Reactivity of Volcanic Ash Using Municipal Solid Incinerator Fly Ash for Alkali-
755 Activated Cement Synthesis.” Waste and Biomass Valorization 11 (2020) 3035–3044.
756 https://doi.org/10.1007/s12649-019-00604-1.

757 U. Hofmann, K. Endell, D. Wilm, Rontgenographishe und kolloidchemishe Untersuchungun
758 uber ton, Angew. Chem. 47 (1934) 539–547

759 Vinai, Raffaele, and Marios Soutsos. 2019. “Cement and Concrete Research Production of
760 Sodium Silicate Powder from Waste Glass Cullet for Alkali Activation of Alternative
761 Binders.” Cement and Concrete Research 116 (June 2018): 45–56.

762 William D. A. Rickard and Arie van Riessen. 2010. Thermal Character of Geopolymers
763 Synthesized from Class F Fly Ash Containing High Concentrations of Iron and a-Quartz.
764 Int. J. Appl. Ceram. Technol., 7 [1] 81–88 (2010) DOI:10.1111/j.1744-
765 7402.2008.02328.x

766 Yankwa Djobo, Jean Noël, Antoine Elimbi, Hervé Kouamo Tchakouté, and Sanjay Kumar.
767 2016. “Mechanical Properties and Durability of Volcanic Ash Based Geopolymer
768 Mortars.” Construction and Building Materials 124: 606–14.

769 Youmoue Martine, Rufin Théophile Tene Fongang, Ameni Gharzouni,·Rodrigue Cyriaque
770 Kaze, Elie Kamseu, Vincenzo M. Sglavo, Ignas Tonle Kenfack, Benoit Nait-Ali, Sylvie
771 Rossignol. 2020. Effect of silica and lignocellulosic additives on the formation and the
772 distribution of meso and macropores in foam metakaolin-based geopolymer filters for
773 dyes and wastewater filtration. SN Applied Sciences (2020) 2:642.

774 Yuan Peng, Peter D. Southon, Zongwen Liu, Malcolm E. R. Green, James M. Hook, Sarah J.
775 Antill, and Cameron J. Kepert. 2008. Functionalization of Halloysite Clay Nanotubes by
776 Grafting with γ-Aminopropyltriethoxysilane. J. Phys. Chem. C 2008, 112, 15742–15751.

Yuan Peng, Daoyong Tan, Faïza Annabi-Bergaya. 2015. Properties and applications of halloysite nanotubes: recent research advances and future prospects. Applied Clay Science 112–113 (2015) 75–93.

Yuan Peng, Daoyong Tan, Fai¨Za Annabi-Bergaya, Wenchang Yan, Mingde Fan, Dong Liu And Hongping He. 2008. Changes in structure, morphology, porosity, and surface activity of mesoporous halloysite nanotubes under heating. Clays and Clay Minerals, Vol. 60, No. 6, 561–573, 2012.

Zhang, Z, H Wang, X Yao, and Y Zhu. 2012. "Cement & Concrete Composites Effects of Halloysite in Kaolin on the Formation and Properties of Geopolymers." *Cement and Concrete Composites* 34 (5): 709–15.

Zhang Baifa, Haozhe Guo, Peng Yuan, Yun Li, Qiang Wang, Liangliang Deng,Dong Liu. 2020. Geopolymerization of halloysite via alkali-activation: Dependence of microstructures on precalcination. Applied Clay Science 185 (2020) 105375.

Figure and table captions

Figure 1. Granulometry of calcined halloysite clays MH600, MH650, MH700 and MH750.

Figure 2. SEM images of raw (HA) and calcined halloysite (MH700) observed at different magnifications (1200x, 3000x and 6000x).

Figure 3. X-ray patterns of calcined halloysite clays MH600, MH650, MH700 and MH750. Key: (Q) (quartz, SiO_2, PDF #5-349); (He) (hematite, Fe_2O_3, PDF #13-5) and (An) (anatase, TiO_2, PDF #4-447).

Figure 4. DTA/TG curves of raw (A) and calcined halloysite (B and C) at 600, 650, 700 and 750 °C.

Figure 5. Infrared spectra of raw halloysite clay (A) and calcined calcined halloysite (B).

800 Figure 6. Isothermal conduction calorimetry plot of alkali activation and heat-evolution
801 released of dissolution of meta-halloysite labelled MH600, MH650, MH700 and MH750 with
802 time.

803 Figure 7. Oscillatory strain sweep at 1 Hz of GPMH600 (A), GPMH650 (B), GPMH700 (C)
804 and GPMH750 (D) meta-halloysite-based geopolymers.

805 Figure 8. Compliance as function of time for fresh meta-halloysite-based geopolymer pastes
806 cured at room temperature at 3600s (A); infrared spectra (B) and DTA/TG curves of (C and
807 D) of consolidated meta-halloysite-based geopolymers.

808 Figure 9. X-ray patterns of hardened meta-halloysite based geopolymers labelled GPMH600,
809 GPMH650, GPMH700 and GPMH750. Key: (Q) (quartz, SiO_2, PDF #5-349); (He) (hematite,
810 Fe_2O_3, PDF #13-5) and (An) (anatase, TiO_2, PDF #4-447).

811 Figure 10. SEM images of meta-halloysite based geopolymers at lower (A) and higher (B)
812 magnification.

813 Table 1. Particle size, specific surface areas and bulk density of calcined halloysite clay
814 MH600, MH650, MH700 and MH750 samples.

815 Table 2. Setting time and physical properties of meta-halloysite based geopolymers.

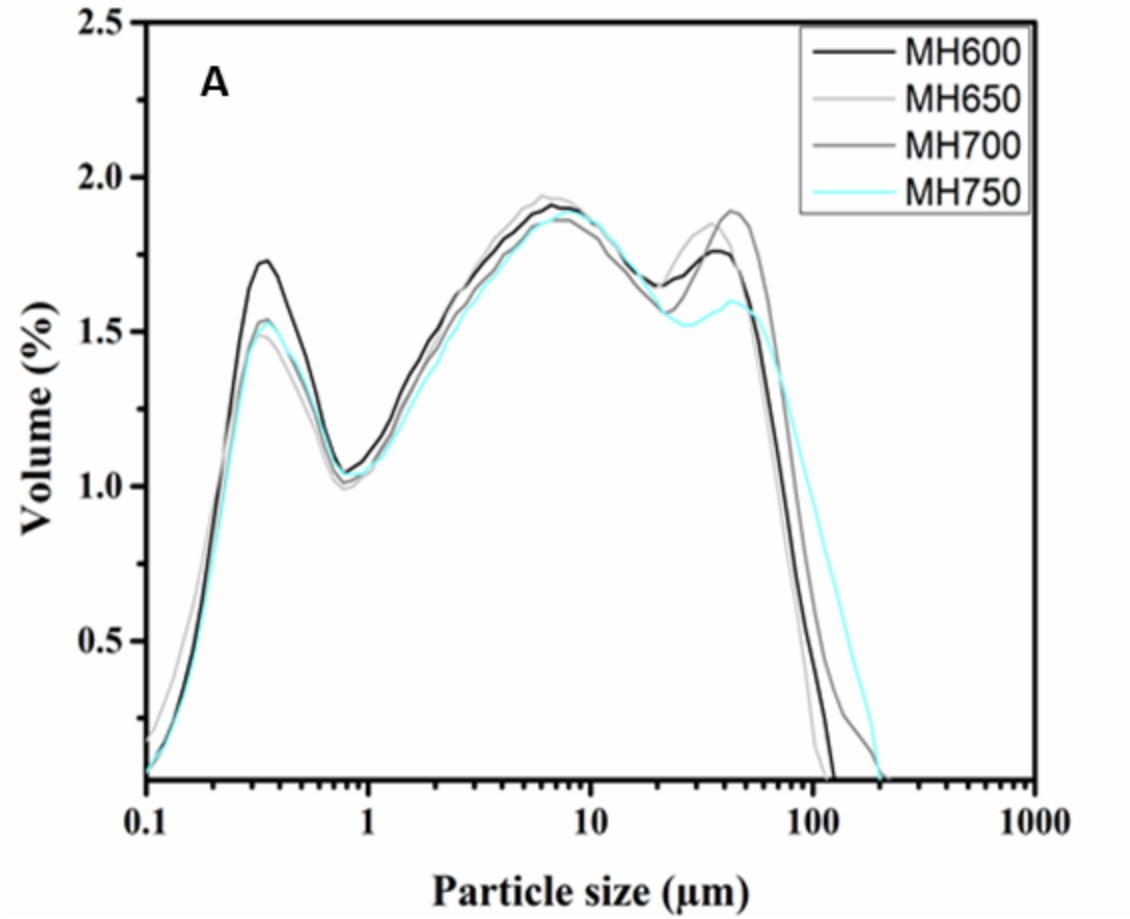
A
MH600
MH650
MH700
MH750
Volume (%)
2.5
2.0
1.5
1.0
0.5
0.1
1
10
100
1000
Particle size (μm)

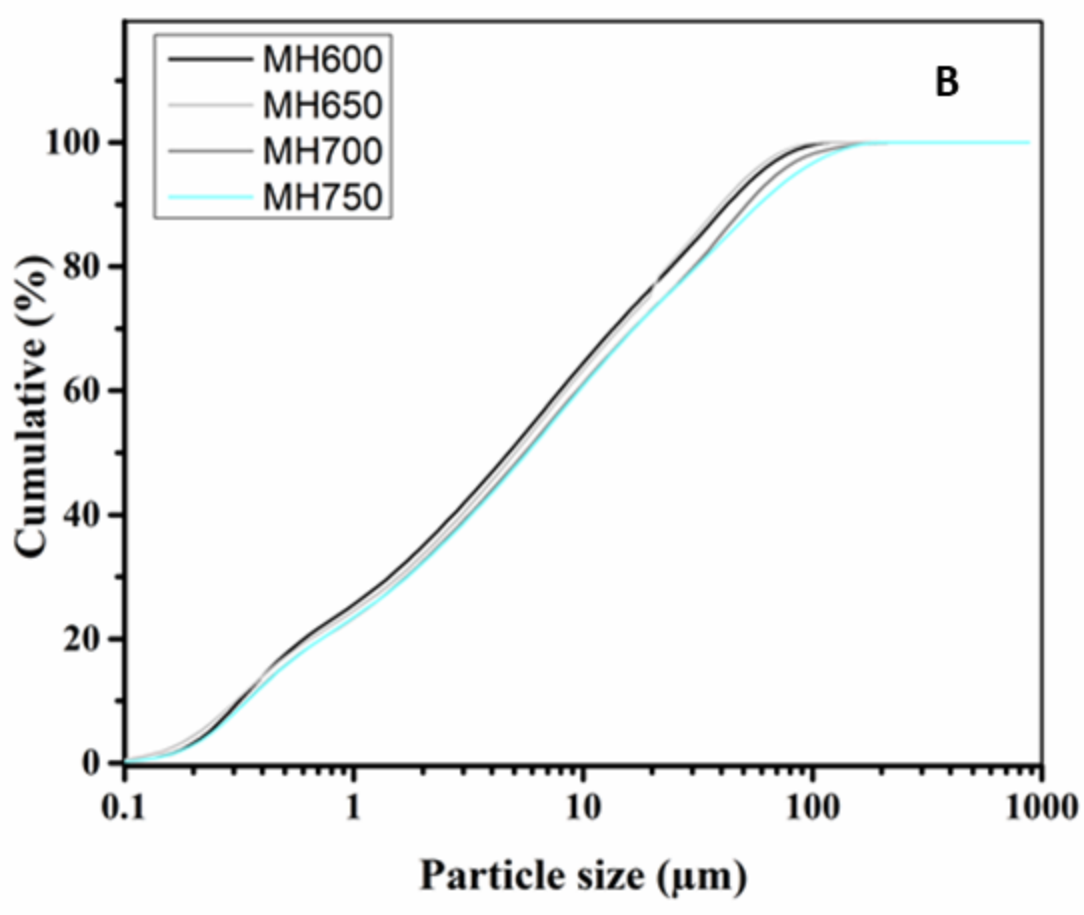
B
MH600
MH650
MH700
MH750
Cumulative (%)
100
80
60
40
20
0
0.1
1
10
100
1000
Particle size (μm)

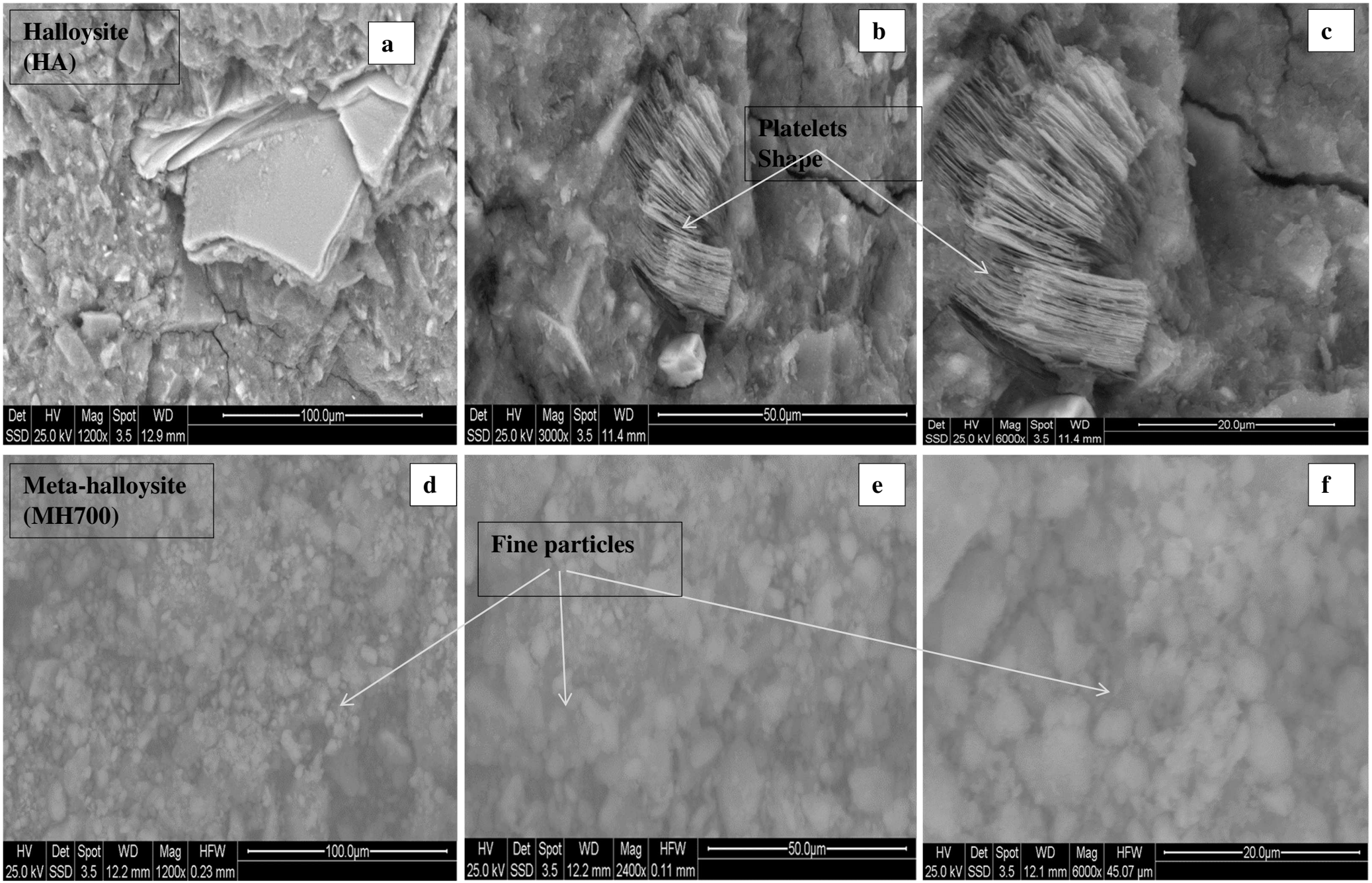
Halloysite
(HA)
a
Det SSD
HV 25.0 kV
Mag 1200x
Spot 3.5
WD 12.9 mm
100.0µm
b
Platelets
Shape
Det SSD
HV 25.0 kV
Mag 3000x
Spot 3.5
WD 11.4 mm
50.0µm
c
Det SSD
HV 25.0 kV
Mag 6000x
Spot 3.5
WD 11.4 mm
20.0µm
Meta-halloysite
(MH700)
d
HV 25.0 kV
Det SSD
Spot 3.5
WD 12.2 mm
Mag 1200x
HFW 0.23 mm
100.0µm
e
Fine particles
HV 25.0 kV
Det SSD
Spot 3.5
WD 12.2 mm
Mag 2400x
HFW 0.11 mm
50.0µm
f
HV 25.0 kV
Det SSD
Spot 3.5
WD 12.1 mm
Mag 6000x
HFW 45.07 µm
20.0µm

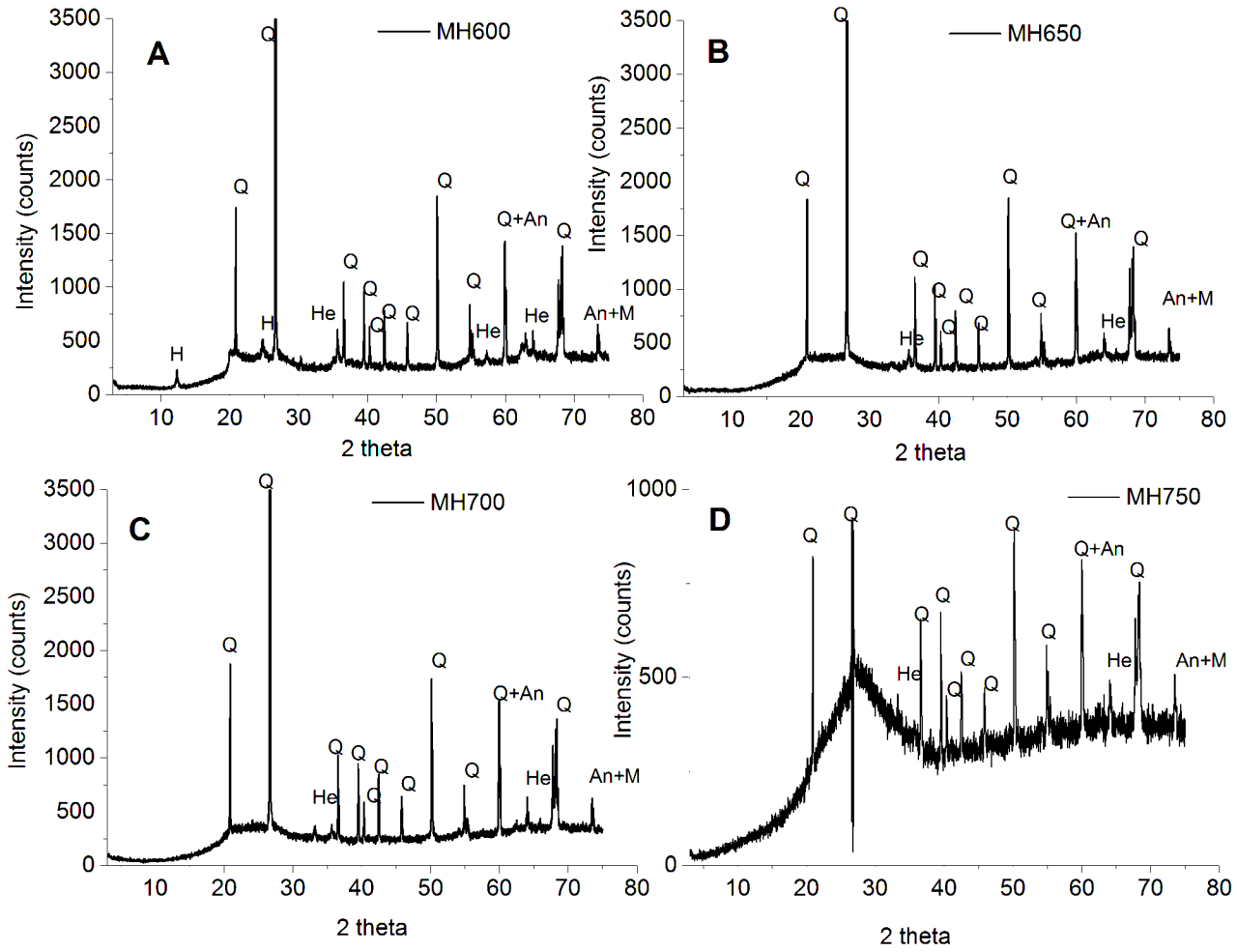
A
MH600
Intensity (counts)
2 theta
H
Q
He
Q+An
An+M
B
MH650
C
MH700
D
MH750

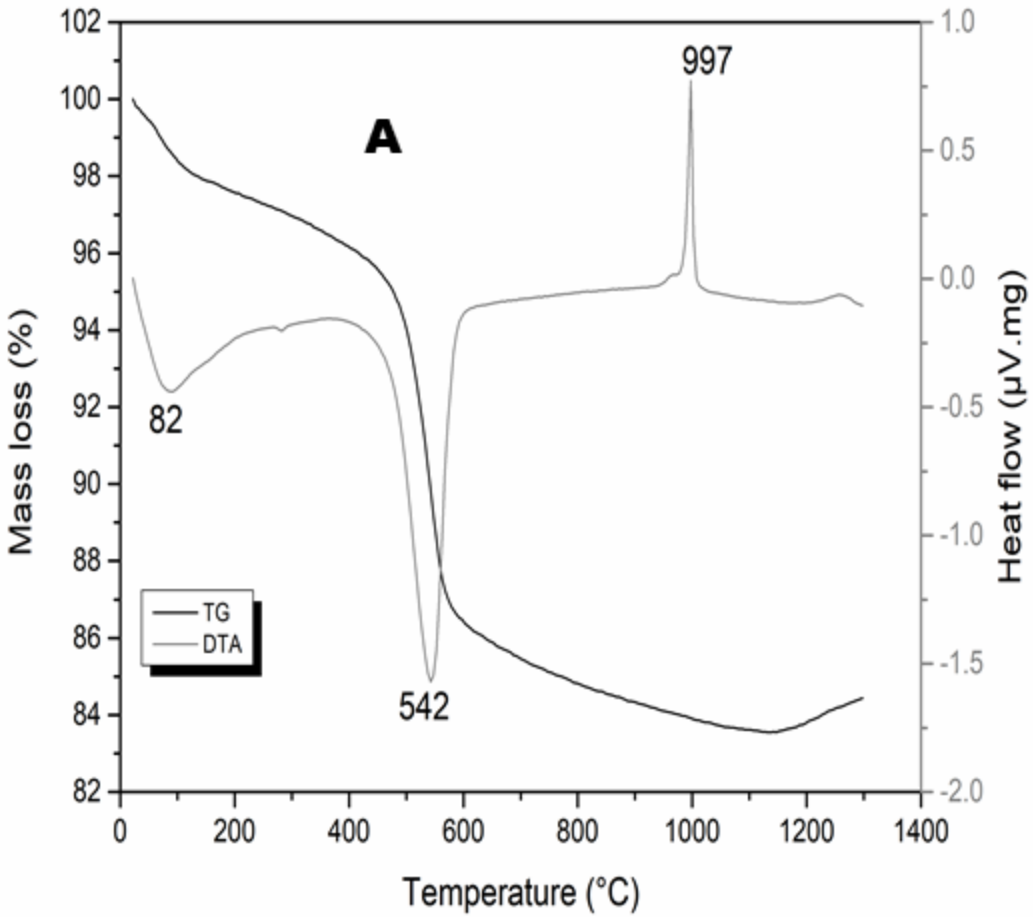
A
Mass loss (%)
Heat flow (µV.mg)
Temperature (°C)
TG
DTA
997
82
542

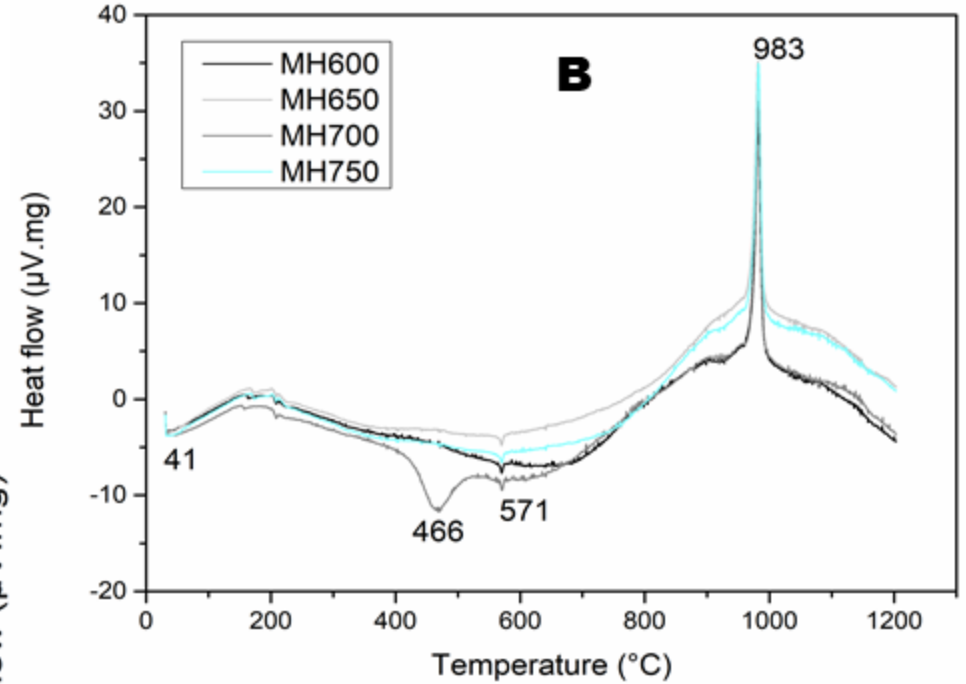
B
MH600
MH650
MH700
MH750
Heat flow (µV.mg)
Temperature (°C)
983
41
466
571

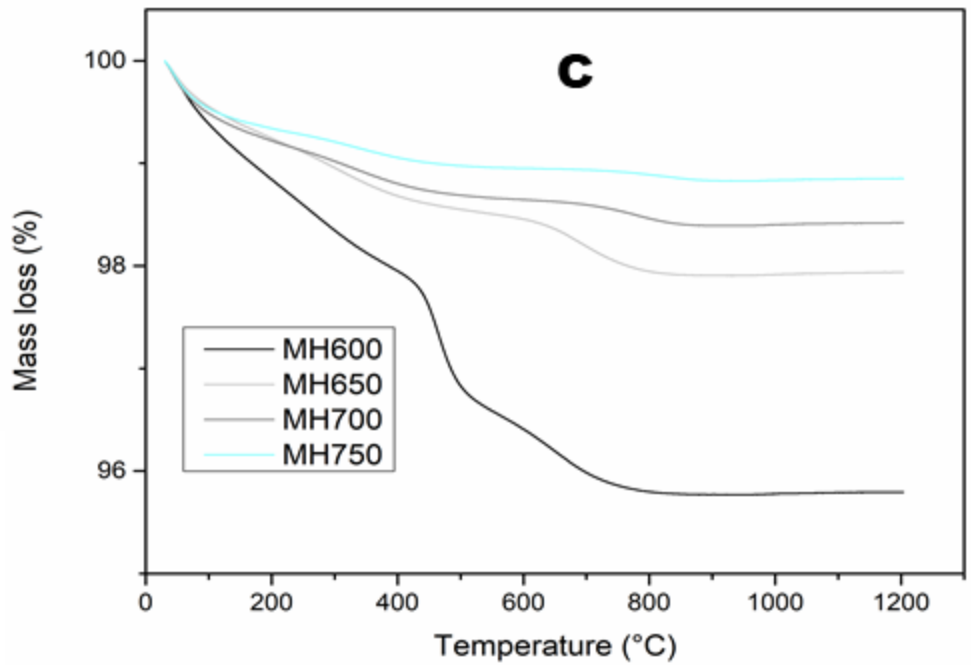
C
MH600
MH650
MH700
MH750
Mass loss (%)
Temperature (°C)

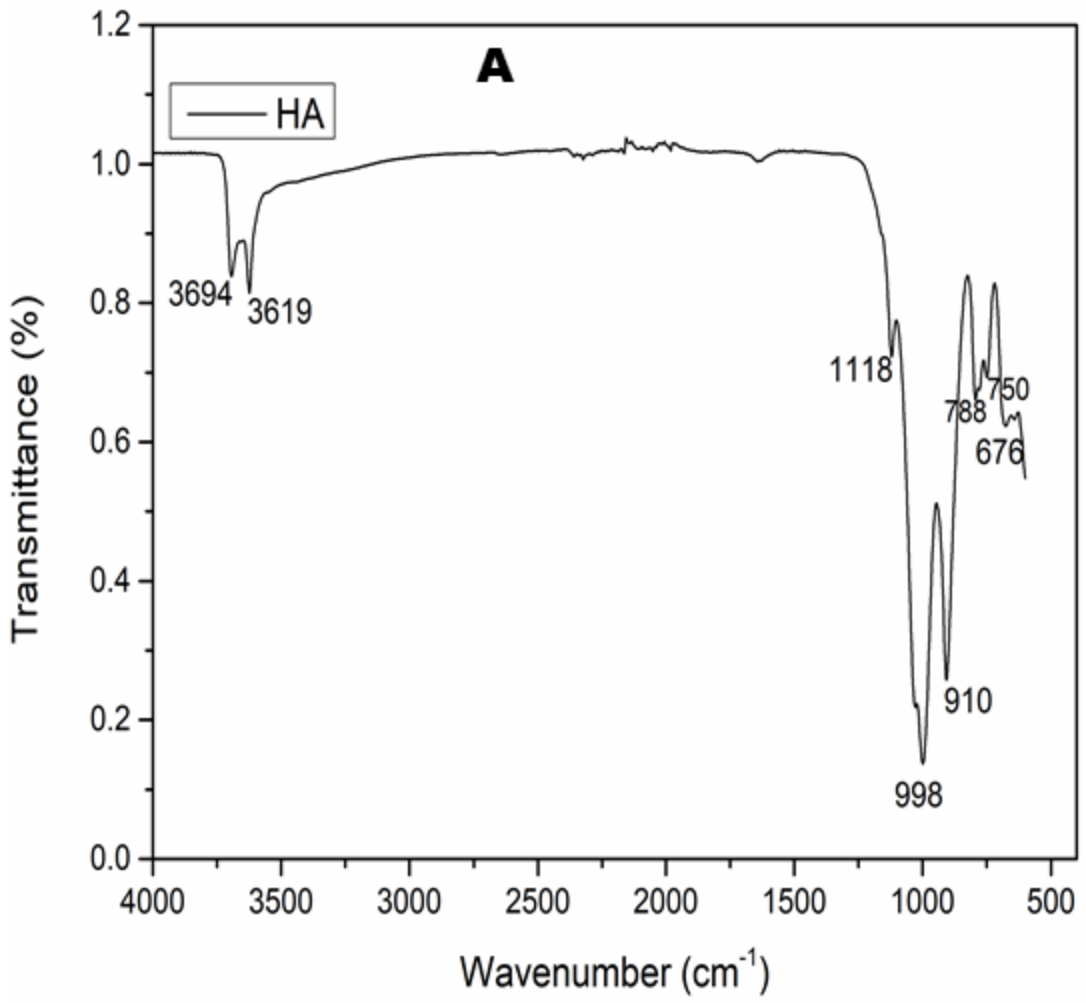
A
HA
Transmittance (%)
Wavenumber (cm-1)
3694
3619
1118
998
910
788
750
676

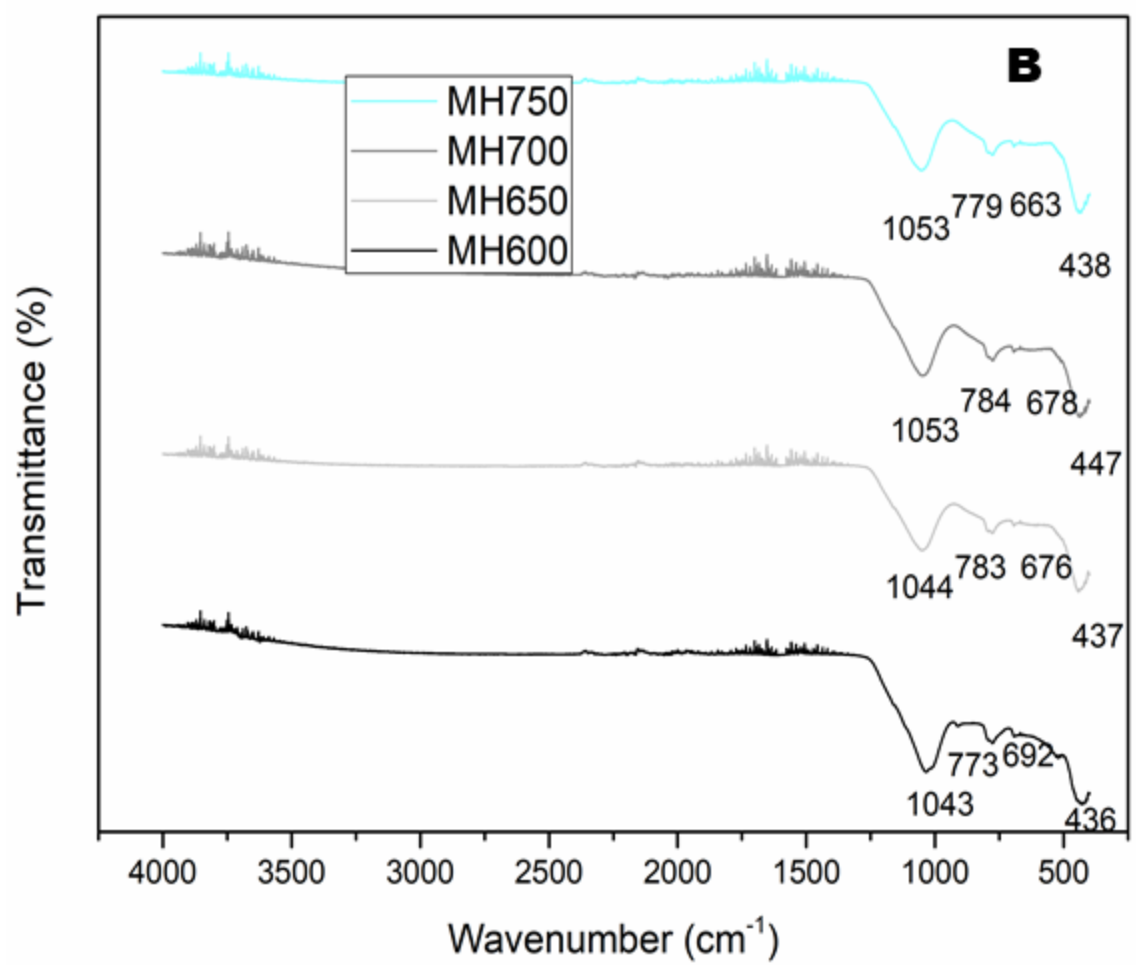
B
MH750
MH700
MH650
MH600
Transmittance (%)
Wavenumber (cm-1)
1053
779
663
438
1053
784
678
447
1044
783
676
437
1043
773
692
436

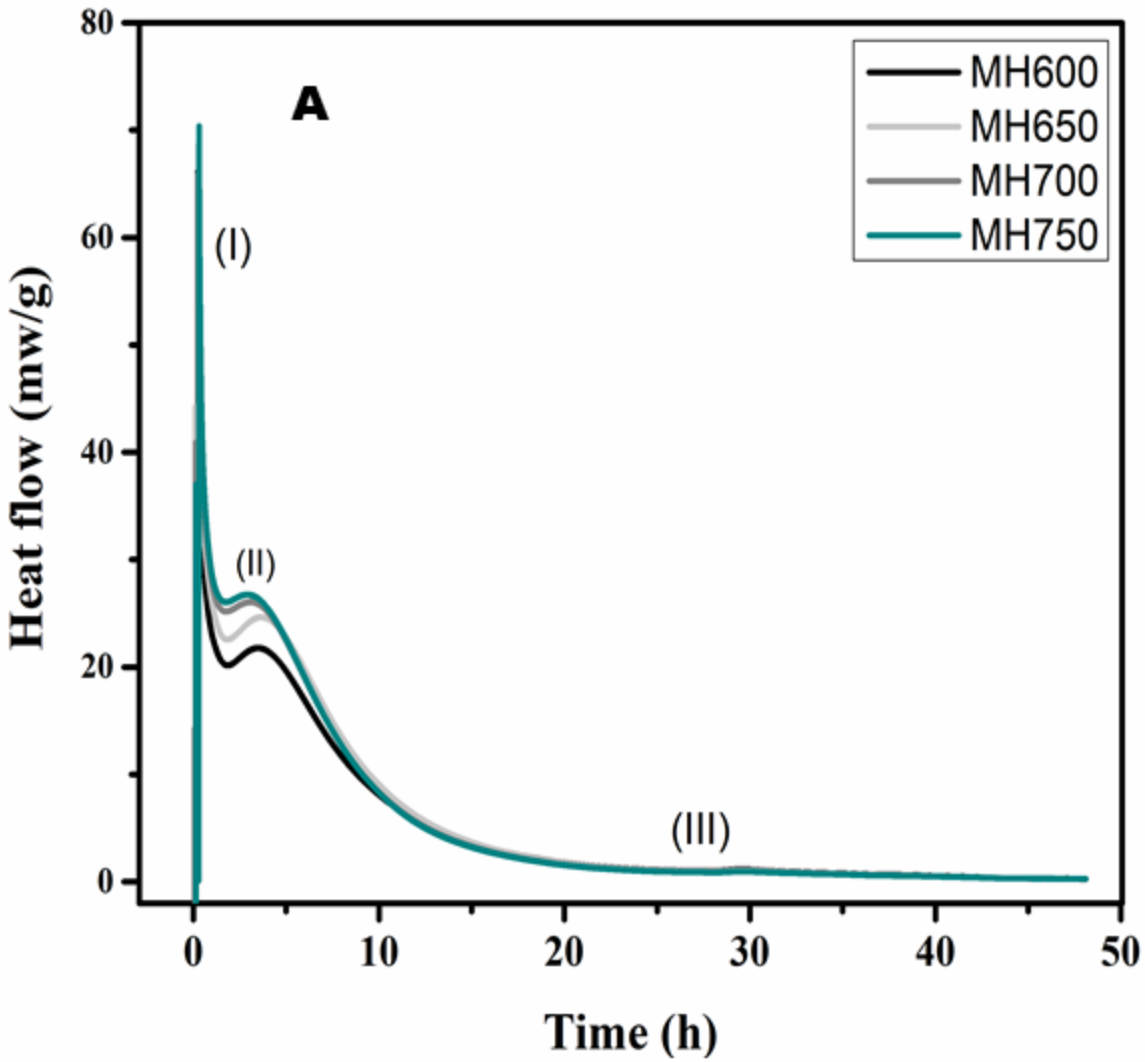
A
MH600
MH650
MH700
MH750
(I)
(II)
(III)
Heat flow (mw/g)
Time (h)
0
20
40
60
80
0
10
20
30
40
50

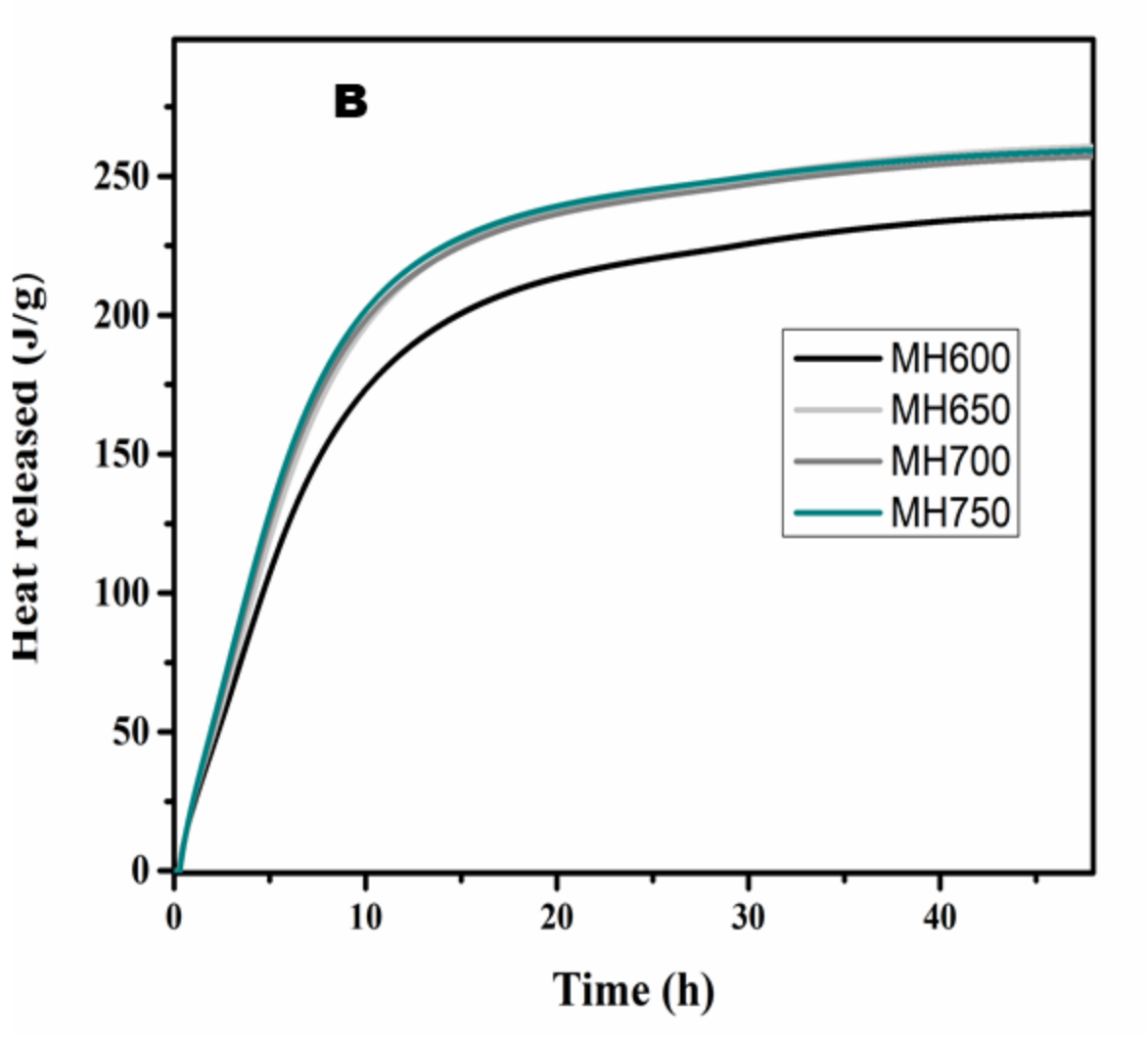
B
MH600
MH650
MH700
MH750
Heat released (J/g)
Time (h)
0
50
100
150
200
250
0
10
20
30
40

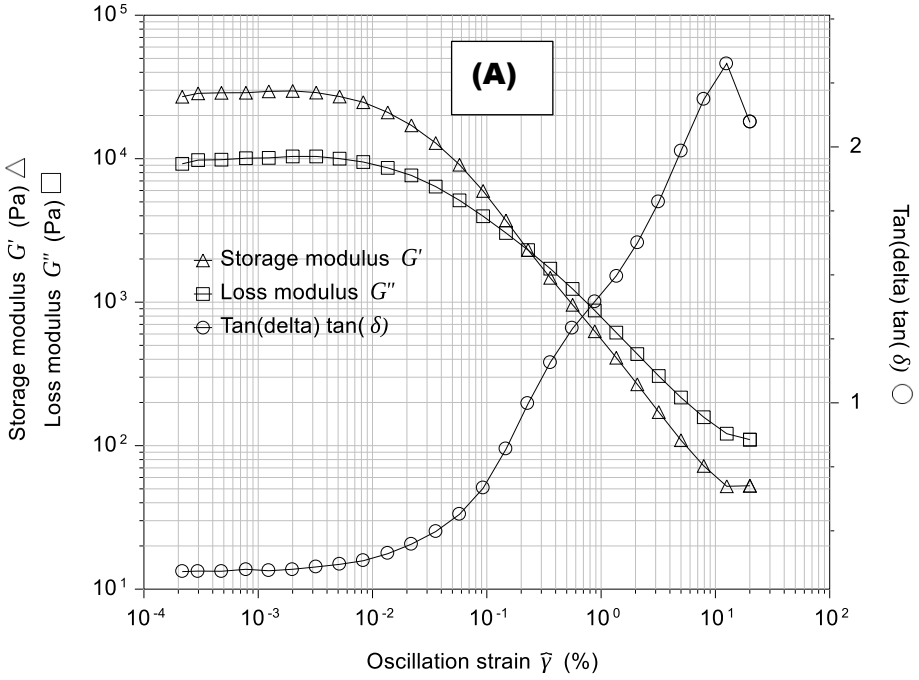
(A)
Storage modulus G′ (Pa) △
Loss modulus G″ (Pa) □
Tan(delta) tan(δ) ○
Storage modulus G′
Loss modulus G″
Tan(delta) tan(δ)
Oscillation strain γ̂ (%)

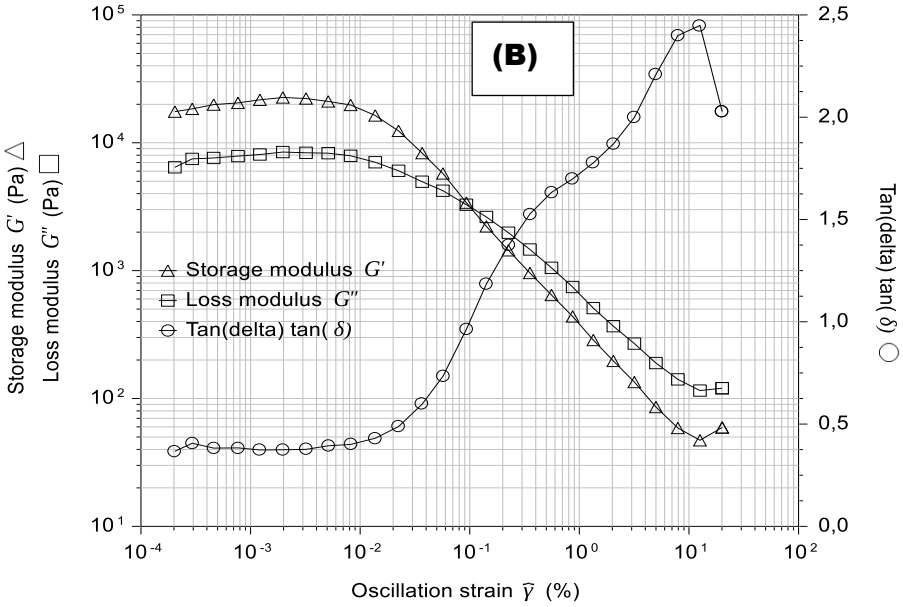
(B)
Storage modulus G′ (Pa) △
Loss modulus G″ (Pa) □
Tan(delta) tan(δ) ○
Storage modulus G′
Loss modulus G″
Tan(delta) tan(δ)
Oscillation strain γ̂ (%)

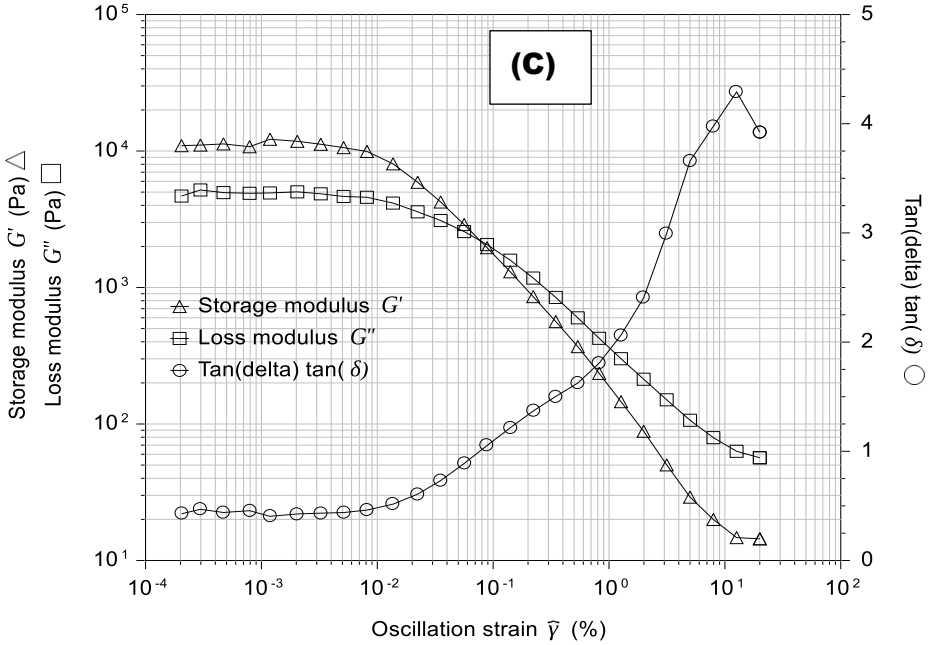
(C)
Storage modulus G′ (Pa) △
Loss modulus G″ (Pa) □
Tan(delta) tan(δ) ○
Storage modulus G′
Loss modulus G″
Tan(delta) tan(δ)
Oscillation strain γ̂ (%)

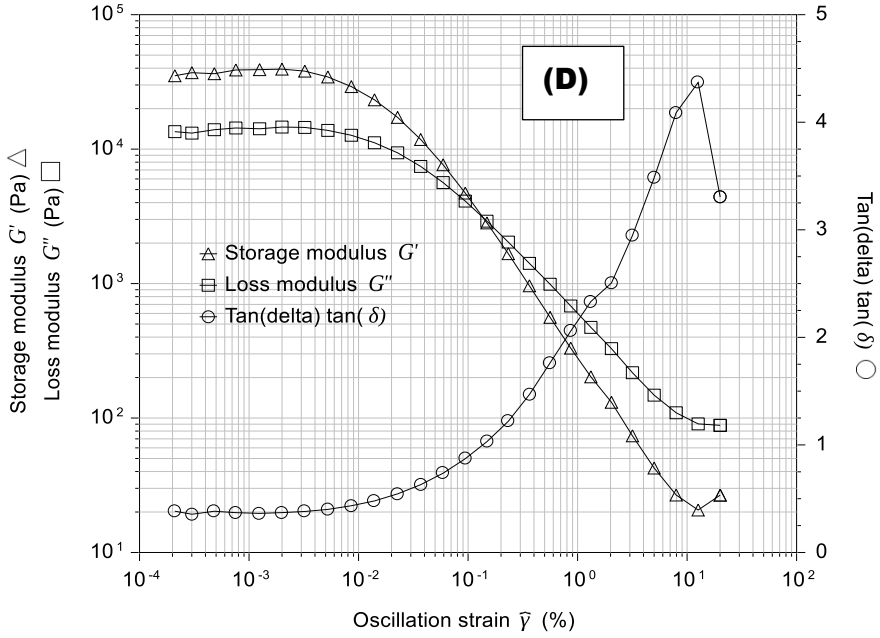
(D)
Storage modulus G′ (Pa) △
Loss modulus G″ (Pa) □
Tan(delta) tan(δ) ○
Storage modulus G′
Loss modulus G″
Tan(delta) tan(δ)
Oscillation strain γ̂ (%)

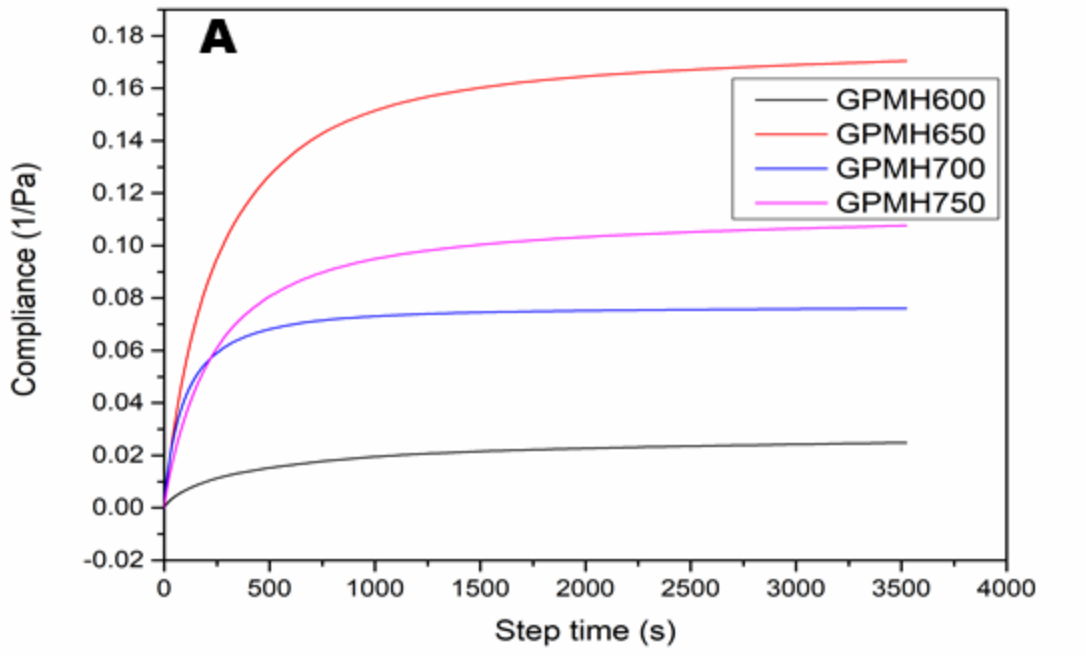
A
Compliance (1/Pa)
Step time (s)
GPMH600
GPMH650
GPMH700
GPMH750

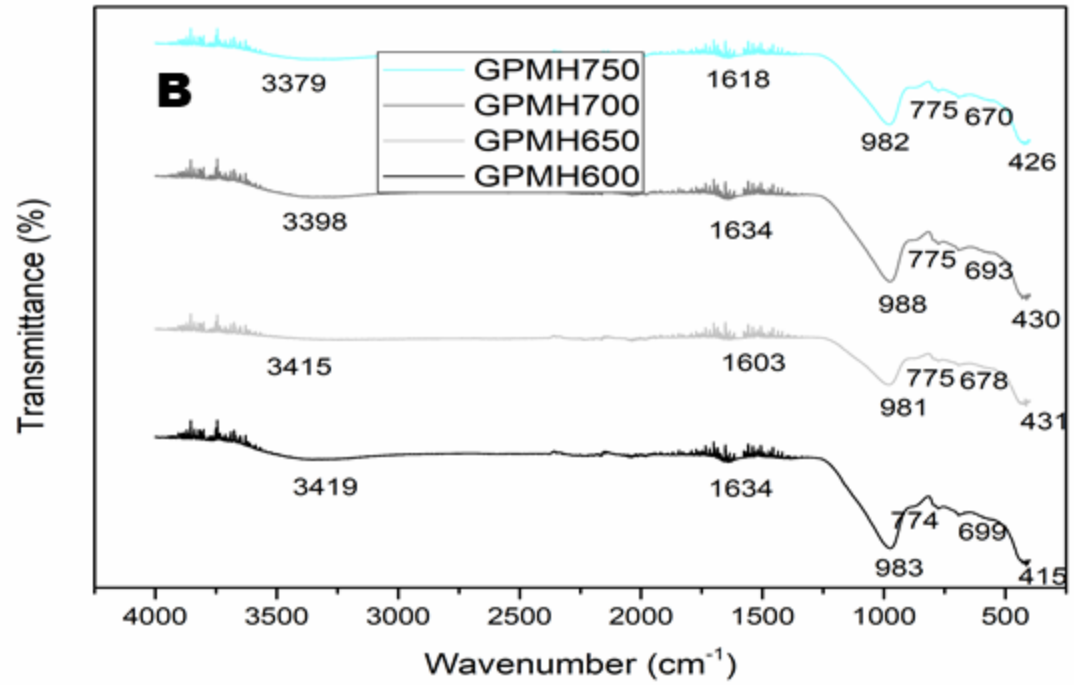
B
Transmittance (%)
Wavenumber (cm-1)
GPMH750
GPMH700
GPMH650
GPMH600
3379
1618
982
775
670
426
3398
1634
988
775
693
430
3415
1603
981
775
678
431
3419
1634
983
774
699
415

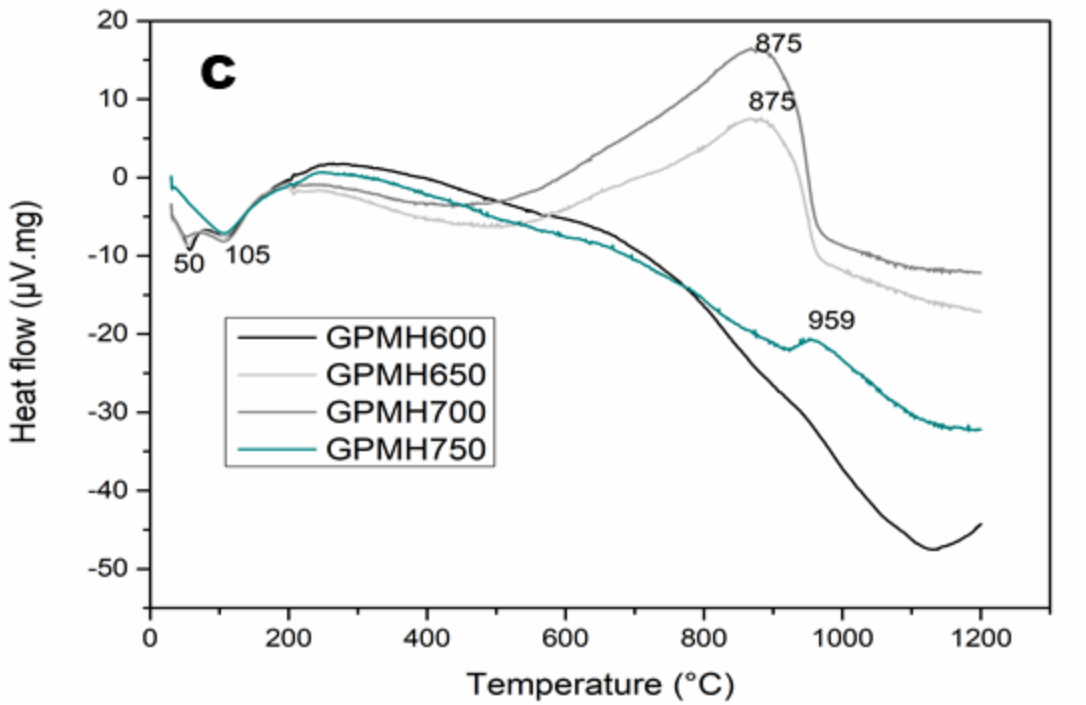
C
Heat flow (μV.mg)
Temperature (°C)
GPMH600
GPMH650
GPMH700
GPMH750
875
875
50
105
959

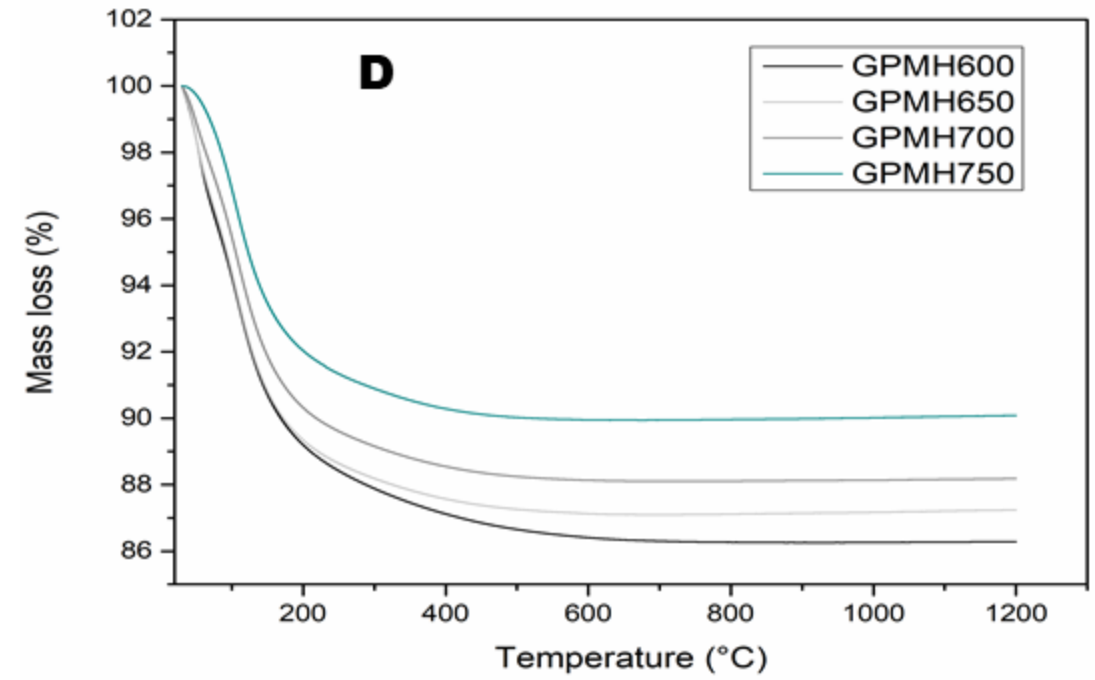
D
Mass loss (%)
Temperature (°C)
GPMH600
GPMH650
GPMH700
GPMH750

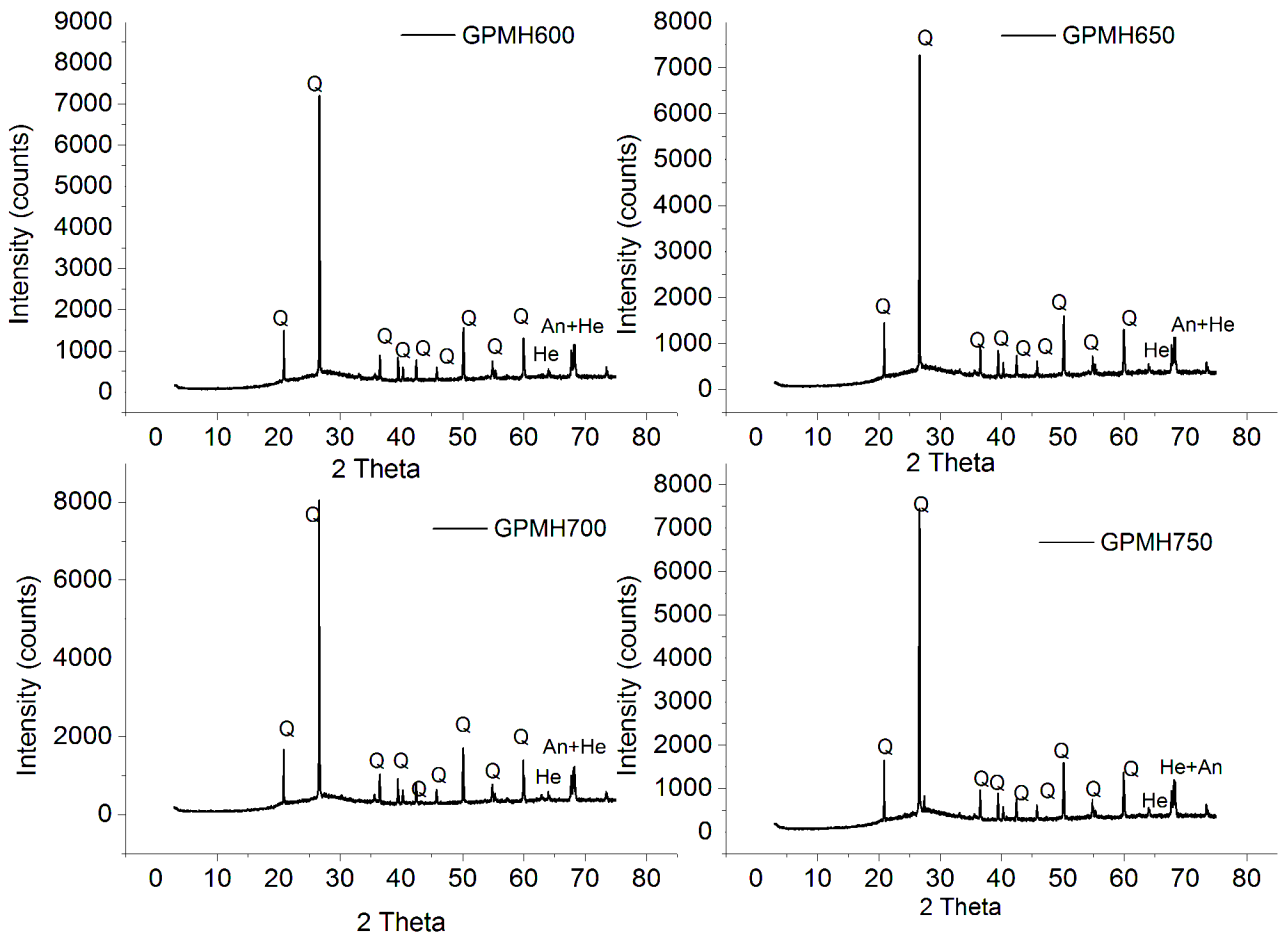
GPMH600
Intensity (counts)
2 Theta
Q
An+He
He
GPMH650
GPMH700
GPMH750
He+An

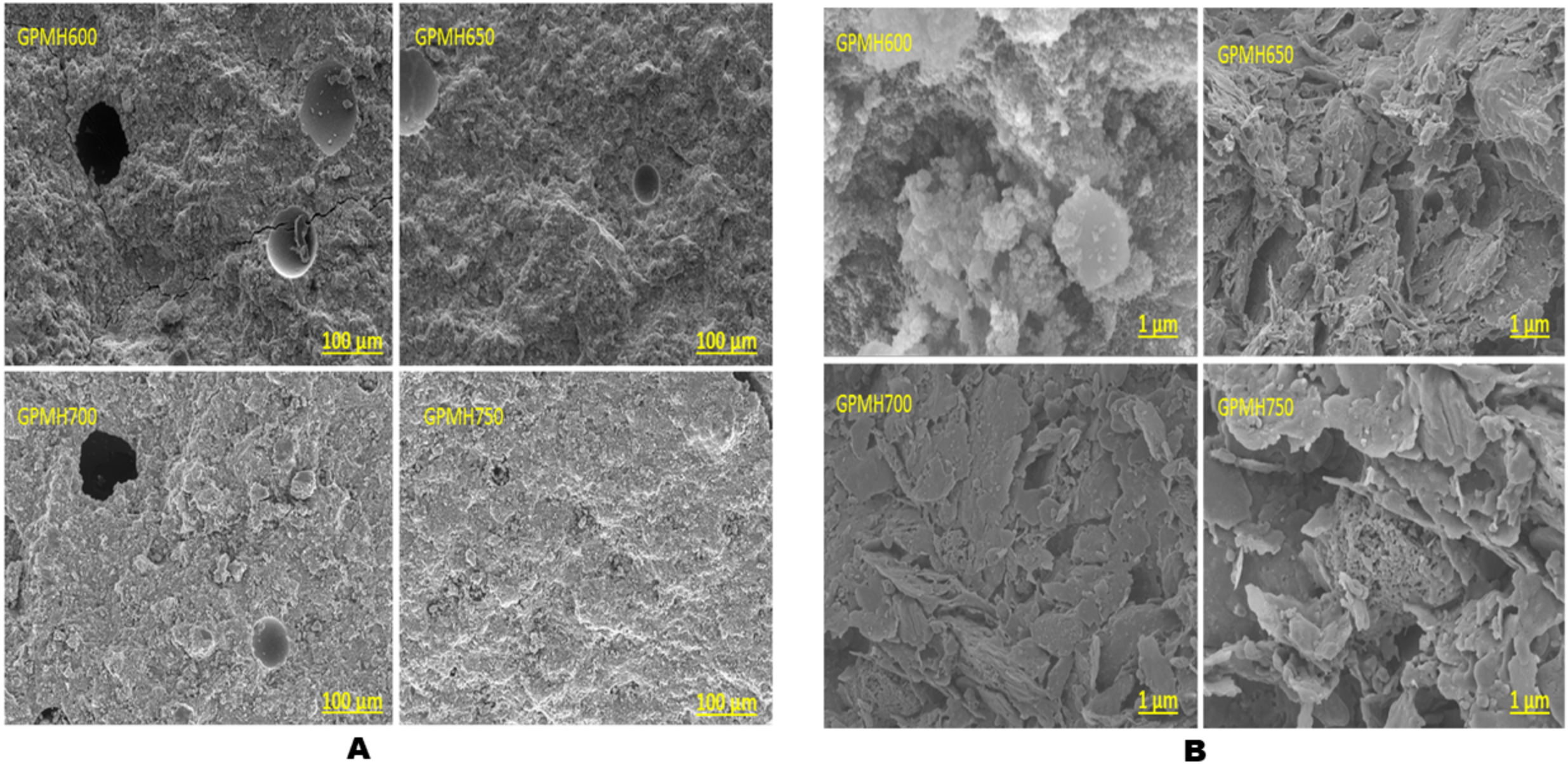
GPMH600
100 µm
GPMH650
100 µm
GPMH700
100 µm
GPMH750
100 µm
A
GPMH600
1 µm
GPMH650
1 µm
GPMH700
1 µm
GPMH750
1 µm
B

Table 1. Particle size, specific surface areas and bulk density of calcined halloysite clay

	Particles size distribution				
Meta-halloysite Samples	$d_{0.1}$ (μm)	$d_{0.5}$ (μm)	$d_{0.9}$ (μm)	B.E.T surface areas (m^2/g)	Bulk density (g/cm^3)
MH600	0.32	4.72	42.53	28.20±0.12	2.82±0.02
MH650	0.31	5.03	43.98	29.52±0.13	2.95±0.02
MH700	0.34	5.54	51.59	25.92±0.11	2.01±0.02
MH750	0.34	5.69	58.29	25.83±0.10	2.01±0.02

Samples	Initial setting time (min.)	Compressive strength (7, 28, 90 and 180 days)				Bulk density (g/cm^3) (7, 28, 90 and 180 days)				Water absorption (%) (7, 28, 90 and 180 days)			
		7	28	90	180	7	28	90	180	7	28	90	180
GPMH600	326	18.30	28.82	31.30	32.30	1.90	1.87	1.67	1.67	24.74	20.23	19.50	18.20
GPMH650	245	28.90	58.40	62.40	66.80	1.97	1.86	1.86	1.86	19.15	15.80	14.62	13.50
GPMH700	196	29.90	61.50	65.50	68.70	1.97	1.86	1.86	1.86	17.23	14.30	10.20	9.23
GPMH750	210	30.23	68.50	70.34	73.70	1.95	1.87	1.87	1.86	16.13	13.40	9.20	10.40